BBA - Molecular Basis of Disease 1865 (2019) 165555

Contents lists available at ScienceDirect

BBA - Molecular Basis of Disease

journal homepage: www.elsevier.com/locate/bbadis

Inactivation of FAM20B causes cell fate changes in annulus fibrosus of mouse intervertebral disc and disc defects via the alterations of TGF-β and MAPK signaling pathways

Wuliji Saiyin[1], Lili Li[1], Hua Zhang, Yongbo Lu, Chunlin Qin*

Department of Biomedical Sciences, Texas A&M University College of Dentistry, Dallas, TX 75246, USA

ARTICLE INFO

Keywords:
FAM20B
Annulus fibrosus
Chondroitin sulfate
Heparan sulfate
TGF-β signaling pathway
MAPK signaling pathway

ABSTRACT

Intervertebral disc (IVD) disorder is often caused by the defect of annulus fibrosus (AF), especially that of the outer AF. Studies about the mechanisms governing the development of the outer AF are needed for a better understanding of pathogenesis of IVD defects. Glycosaminoglycans (GAGs) are essential components of extracellular matrix (ECM) in AF. FAM20B is a newly identified xylose kinase that catalyzes the biosynthesis of GAGs. In this study, we created *Fam20B* conditional knockout (cKO) mice in which FAM20B was inactivated in type I collagen-expressing cells, the main type of cells in the outer AF of IVD. The cKO mice showed severe spine deformity and remarkable IVD defects associated with AF malformation. The AF of cKO mice had a lower level of chondroitin sulfate and heparan sulfate, and the outer AF cells lost their normal fibroblast-like morphology and acquired chondrocyte phenotypes, expressing a higher level of Sox 9 and type II collagen along with a reduced level of type I collagen. The level of phospho-Smad 2 and phospho-Smad 3, and that of scleraxis, a downstream target molecule of canonical TGF-β signaling pathway were significantly lower in the AF of cKO mice. The AF in cKO mice also manifested altered levels in the molecules associated with the activations of MAPK pathway; the changes included the increase of phospho-P38 and phospho-ERK and a decrease of phospho-JNK. These results indicate that FAM20B plays an essential role in the development of AF by regulating the TGF-β signaling and MAPK signaling pathways.

1. Introduction

Intervertebral disc (IVD) disorder is a worldwide health problem causing serious social and economic burden [1]. While IVD lesion can be attributed to a broad spectrum of factors such as aging, smoking, infection, abnormal mechanical stress, diabetes, trauma, and genetic predisposition [2], its treatment options are quite limited, primarily aimed at relieving the symptoms rather than complete eradication; these therapeutic limitations are, in part, due to a relatively poor understanding of the mechanisms governing the development of IVD and the pathogenesis of its defects. The developmental defects of the three IVD substructures, the central nucleus pulposus (NP), the peripheral annulus fibrosus (AF), and the superior and inferior endplates (EP), make the IVD prone to degeneration and destruction [3–5]. While the relationship between NP/EP defects and IVD degeneration/destruction has been well studied [6–9], there has been very little information regarding the relationship between IVD defects and AF development.

AF is a multi-lamellar collagen-rich fibrocartilage tissue surrounding NP [10]. The extracellular matrix (ECM) of AF plays an important role in the development and maintenance of AF [11,12]. The major components of AF ECM are collagens (60%–70% of dry weight, mostly type I collagen) and proteoglycans (15%–20% of dry weight) [13]. Glycosaminoglycans (GAGs), which are covalently linked to amino acids in proteins to form proteoglycans, are important ECM components in AF [14]. GAGs are highly negatively-charged molecules that attract cations and water molecules to sustain compressive and tensile strength from the adjacent vertebral body [15]. As GAGs are vital for the normal structure and functions of AF, the enzymes catalyzing the formation of GAGs are believed to be essential to the development of AF [16].

FAM20B (family with sequence similarity 20, member B) is a recently identified xylose kinase, which greatly facilitates the biosynthesis of chondroitin sulfate (CS) and heparan sulfate (HS) [17,18]. FAM20B phosphorylates the initial xylose residue in the tetrasaccharide

* Corresponding author at: Department of Biomedical Sciences, Texas A&M University College of Dentistry, 3302 Gaston Ave, Dallas, TX 75246, USA.
E-mail address: CQin@tamhsc.edu (C. Qin).
[1] These authors contributed equally to this work.

https://doi.org/10.1016/j.bbadis.2019.165555
Received 30 May 2019; Received in revised form 5 September 2019; Accepted 7 September 2019
Available online 09 September 2019
0925-4439/

linkage of CS and HS chains; the attachment of phosphates to this five-carbon sugar is essential to the elongation of CS and HS chains [17–19]. Studies have shown that the constitutive deletion of *Fam20B* in mice leads to embryonic lethality at E13.5 [20], and that the conditional ablation of *Fam20B* in the dental epithelium of mice using *K14-Cre* recombinase leads to supernumerary incisors, and inactivation of mouse *Fam20B* by *Osr2-Cre* recombinase causes chondrosarcoma and postnatal ossification defects in the joint cartilage via the alterations of the WNT, BMP, and PTHrP/IHH signaling pathways [21,22]. These results suggest that FAM20B plays an important role in the development of the organs and tissues via regulating the balanced networks of multiple signaling pathways.

Transforming growth factor β (TGF-β) signaling pathway is involved in many cellular processes in both developing embryos and adult organs; they participate in the growth, differentiation, apoptosis, and homeostasis of cells [23]. It has been well documented that the TGF-β signaling pathways play important roles in the development of AF. Baffi et al. reported that the nullification of the TGF-β signaling pathways led to a size reduction or complete loss of AF [24,25]. Bashar et al. also illustrated that the TGF-β signaling pathways are important for the development of AF [26,27]. Mitogen activated protein kinase (MAPK) signaling pathway can be activated by a variety of extracellular and intracellular stimuli [28] and may regulate numerous cellular activities including proliferation, differentiation, survival, and death [29]. Studies have shown that MAPK signaling pathway participates in the development of AF in IVD and are important for the normal differentiation of AF cells [30,31].

Proteoglycans are known to regulate organogenesis via the modulation of multiple signaling pathways including TGF-β and MAPK pathways [32–34]. FAM20B catalysis is essential to the biosynthesis CS and HS [35], two key constituents of many proteoglycans [36,37]. Therefore, it is reasonable to envision that FAM20B may regulate the development and maintenance of AF through these pathways; this is a research area to which no attention has been given.

In this study, we inactivated FAM20B in type I collagen-expressing cells in mice; in AF, the type I collagen-expressing cells are the main type of cells. Using these *Fam20B* conditional knockout (cKO) mice, we analyzed the effects of FAM20B inactivation on the development of AF and assessed the levels of molecules associated with the activation of TGF-β and MAPK signaling pathways in the AF of the mouse IVD. The cKO mice exhibited severe AF malformation with abnormal differentiation and proliferation of AF cells, along with altered levels of molecules associated with the activation of TGF-β and MAPK pathways. The findings in this investigation indicate that FAM20B inactivation resulted in a transformation of the normal fibroblast-like cells into chondrocytes in the outer AF and this cell fate change, a major contributor to the IVD malformation, may be related to the alterations in TGF-β and MAPK signaling pathways associated with the loss of FAM20B function in the AF cells.

2. Materials and methods

2.1. Generation of 2.3 kb Col I-Cre;Fam20B$^{flox/flox}$ (cKO) mice

The *2.3 kb Col I Cre;Fam20B*$^{flox/flox}$ (cKO) mice were generated by mating *2.3 kb Col 1a1-Cre* mice [38,39] with *Fam20B*$^{flox/flox}$ mice [21,22]. The age- and sex-matched *Fam20B*$^{flox/flox}$ littermates were used as normal controls; these mice showed normal development [22]. Tail biopsies were analyzed by polymerase chain reaction (PCR) genotyping with primers specific for the *Cre* transgene and *Fam20B*-floxed allele, as previously described [21]. We did not observe significant phenotypic differences in the spine and IVDs between the male and female cKO mice. All animal procedures were approved by the Institutional Animal Care and Use Committee (IACUC) of Texas A&M University College of Dentistry (Dallas, TX, USA) and performed in accordance with the National Institutes of Health Guide for the Care and Use of Laboratory Animals.

2.2. Gross observation and X-ray radiography

12 male mice (6 from control group and 6 from cKO group) were photographed and weighed at birth and at 1-, 2-, 3-, 6-and 12-weeks after birth to monitor the body sizes of the animals. For plain X-ray radiography (Faxitron MX-20DC12 system; Faxitron Bioptics, Tucson, Arizona, USA) analyses of the whole skeleton, 12-week-old male mice (6 from each group) were scanned and representative images were shown. For the X-ray analyses of spines, the spines dissected from 3-week-old male mice (at least 3 mice for each group) were imaged.

2.3. Histological analyses

The spines dissected from the embryonic 16.5 (E 16.5) days, newborn, 1-week- and 3-week-old mice were immediately immersed in 4% paraformaldehyde in phosphate-buffered saline (pH 7.4). After an overnight fixation at 4 °C, the samples were then decalcified in 15% ethylenediaminetetraacetate (EDTA) solution (pH 7.4). The decalcification time varied from 2 to 7 days, depending on the age of mice. Then, the samples were processed for paraffin embedding, and 5-μm serial sections were prepared. The paraffin sections were used for Hematoxylin and Eosin (H&E) staining, toluidine blue staining, picro-sirius red staining, immunohistochemistry (IHC) staining, In situ hybridization (ISH), or bromodeoxyuridine (5-bromo-2′-deoxyuridine, BrdU) staining as we previously described [22,40]. For H&E, toluidine blue, picro-sirius red, IHC staining and ISH analyses, at least 3 mice from each group were assessed and multiple sections from the specimen of each mouse were evaluated. For BrdU analyses, 6 mice from each group were examined and multiple sections from each mouse were assessed.

We measured the height of EP in the H&E stained sections from 1-week and 3-week-old control and cKO mice (3 mice from each group at each time point). Twenty points of EP (10 for the upper EP and 10 for lower EP) in the mid-coronal sections from each of the mice (3 mice per group) were selected and the EP heights at each point were measured to calculate the average value.

For toluidine blue staining, the spines dissected from 3-week-old mice were processed for paraffin sections. The sections were incubated in 0.04% toluidine blue (pH 2.0–2.5) at 25 °C for 5 min the samples were washed with two changes of double distilled water and followed by dehydration in gradient ethanol, cleared in xylene and mounted with permount mounting medium for observation.

For picro-sirius red staining, the specimens same as those used for toluidine blue staining were employed to make sections. The sections were stained with hematoxylin solution for 8 min and washed with double distilled water for 10 min, the samples were immersed in picro-sirius red for 1 h followed by washing in two changes of acidified water. Then, the sections were dehydrated in three changes of 100% ethanol, cleared in xylene and mounted. The stained sections were observed under microscopy with polarized light to analyze the structure and organization of collagen fibers in IVD.

For BrdU staining, two doses of BrdU (100 μg/g mouse, Sigma-Aldrich) were administrated via intraperitoneal injections; the first injection was 24 h and the second injection was 2 h before sacrifice at postnatal 3 weeks. The spines were dissected and processed for paraffin sectioning as described above. Then, the BrdU-labeled cells were detected using a BrdU staining kit (Invitrogen) following the manufacturer's instruction. Images of the AF areas were captured under an Olympus BX51 digital camera system and BrdU positive nuclei and total nuclei in the AF area were counted. The ratios of BrdU-labeled cells to total AF cells were calculated to serve as an index of the cell proliferation rate.

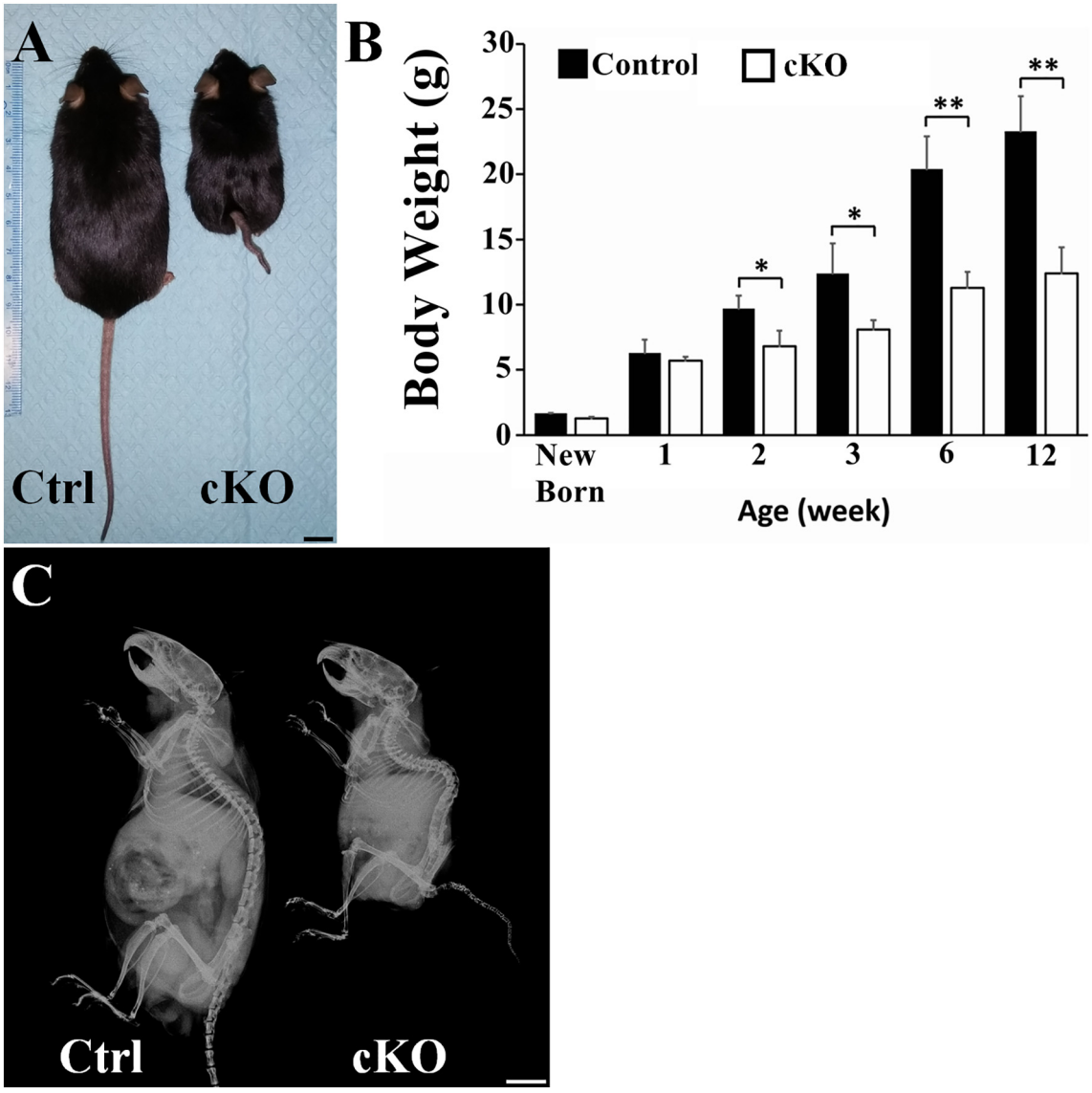

Fig. 1. Inactivation of FAM20B caused growth retardation and spine deformity. (A) Gross pictures of 12-week-old control and cKO male mice (representative photographs out of 6 mice for each group). The cKO mouse was significantly smaller than the control mouse (Bar = 1 cm). (B) The body mass of cKO mice was compared to the normal mice; at each time point, the average body weights were calculated from the measurements of 6 mice (n = 6, *, $p < 0.05$; **, $p < 0.01$). There were no significant differences in the body weights of newly born and 1-weel-old control mice versus cKO mice. Since postnatal two weeks, the body weights of the cKO mice were significantly lower than the age-matched control mice. (C) Skeletal radiography of whole body of 12-week-old control and cKO mice (representative X-ray images out of 6 mice for each group). The spine of the cKO mice is shorter than that of control mouse and the curvature of spine in cKO mice is changed showing kyphosis.

2.4. TUNEL staining

For terminal deoxynucleotidyl transferase-mediated dUTP nick end labelling (TUNEL) staining, the spines from 3-week-old mice were fixed overnight at 4 °C with 4% paraformaldehyde, then in 0.1% diethyl pyrocarbonate (DEPC)-treated 15% EDTA solution at 4 °C for 7 days. Samples were dehydrated with 30% sucrose and embedded in optical coherence tomography (OCT) compound (Sakura Finetek Inc., Torrance, USA). Sections were cut at 5 μm on a cryostat (2800 FRIGOCUT; Leica). The TUNEL analysis was performed using an Apoptag®Plus Fluorescein In Situ Apoptosis Detection kit (EMD Millipore Corporation, Billerica, USA) according to the manufacturer's instructions. Briefly, the sections were washed with PBS and placed in an equilibration buffer for 2 min at room temperature. Subsequently, the slides were incubated with TUNEL reaction mixture that contains the enzyme (TdT) and fluorescent label (tetramethlyrhodamine-conjugated nucleotides) in a humidified chamber for 1 h at 37 °C in the dark. After washing with PBS, the slides were mounted with DAPI (Sigma, California, USA). SP5 Leica confocal microscope was used to capture the fluorescent cell images. The positive signals for the cell apoptosis staining was in green color and DAPI staining was in blue color. The experiments were performed with at least three biological replicates (3 mice) and 3 sections per replicate.

2.5. Alizarin red/alcian blue staining

The 3-week-old control and cKO mice (at least 3 mice from each group) were sacrificed, skinned, eviscerated and fixed in 95% ethanol. Alizarin red/alcian blue staining was performed as in our previous studies to visualize the IVD and the adjacent vertebral body [22].

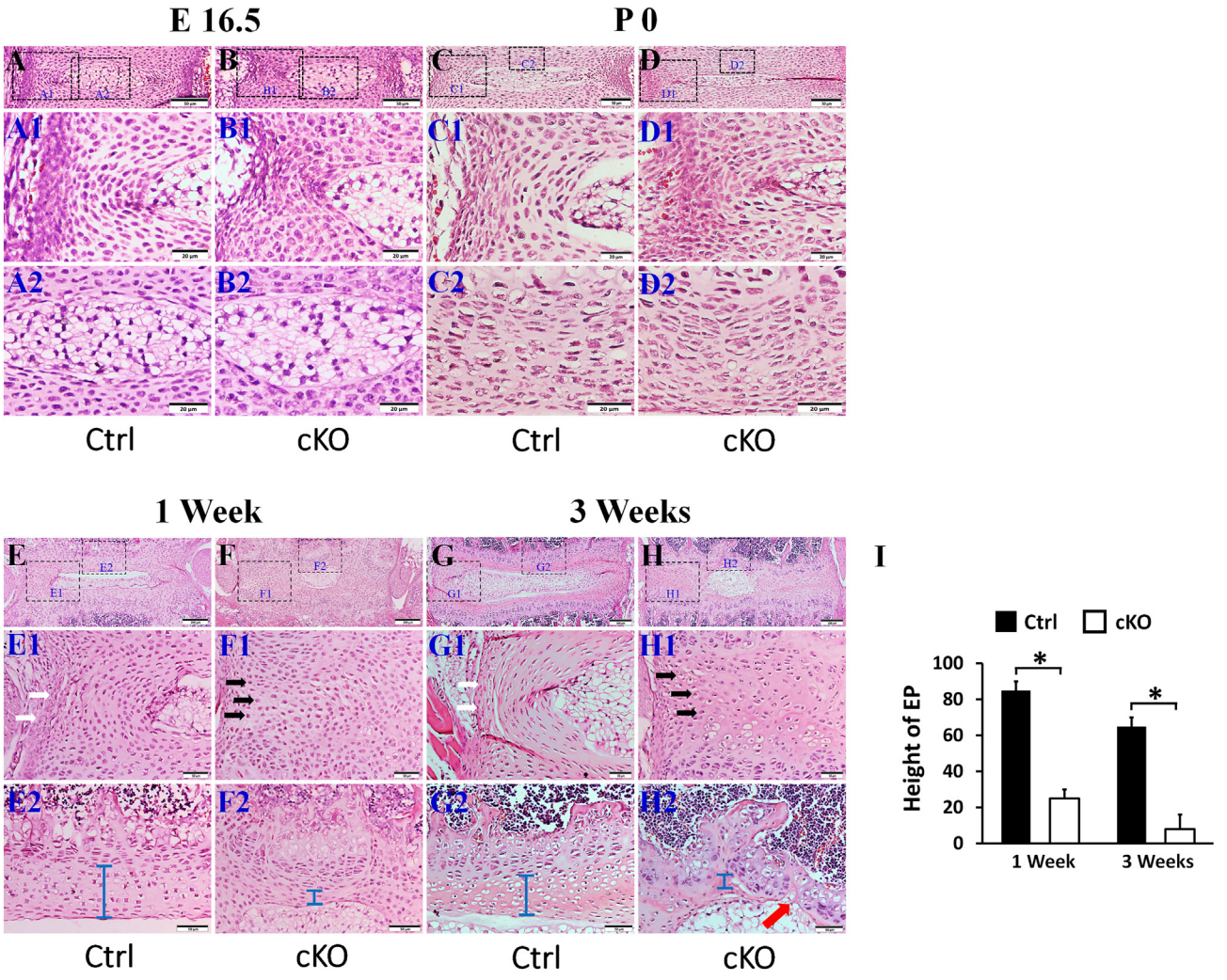

Fig. 2. Inactivation of FAM20B caused abnormalities in IVD. H&E staining of mid-coronal (A, B, C, D, E, F, G, H) sections of L3 lumber IVDs of control mice and cKO mice (representative images of at least 3 mice for each group). A1, B1, C1, D1, E1,F1, G1 and H1 were the higher magnification views of larger (left) boxes in A, B, C, D, E,F, G, and H, respectively; A2, B2, C2, D2, E2,F2, G2, and H2 were the higher magnification views of smaller (right) boxes in panels A, B, C, D, E, F, G and H, respectively (Bars in the A, B, C, D, E1, F1, G1, H1, E2, F2, G2, H2 = 50 μm, Bars in the E, F, G, H = 200 μm). (I) Average EP heights in the IVDs of 1-week-old and 3-week-old mice (n = 3). The cKO mice at E 16.5 days and at birth showed mildly malformed IVD, with the AF cells became bigger and rounder. In the 1- and 3-week-old cKO mice, the size of the NP was remarkably smaller and the EP (blue bar) was apparently thinner than the age-matched control mice; in some areas the EP was completely lost (red arrow in H2). The AF cells in 1- and 3-week-old cKO mice lost their normal morphology of spindle shaped cells (white arrows) and were replaced by the rounder chondrocyte-like cells (black arrows).

2.6. Immunohistochemistry (IHC) and immunofluorescence (IF) staining

The IHC experiments on paraffin-embedded sections were carried out using ABC kit and DAB kit (Vector Laboratories, Burlingame, California, USA) according to the manufacturer's instructions, and as previously described [40]. Briefly, paraffin sections from 3-week-old mice were dewaxed and rehydrated and then treated with 3% H_2O_2 to block endogenous peroxidase activity followed by heat-induced antigen retrieval in citrate buffer. Then, sections were incubated with 3% bovine serum albumin and 10% normal goat or normal rabbit serum to block nonspecific reactions. Sections were then incubated with primary antibodies overnight at 4 °C. Next, sections were incubated with biotinylated secondary antibodies at room temperature for 1 h. Finally, sections were treated with ABC kit (Vector, PK-6100), and the immunoreactivity was visualized by adding 3, 3′-diaminobenzidine tetrahydrochloride (DAB) solution (Vector, SK-4100), with positive signals being in brown color. Sections were counterstained with methyl green solution. Primary antibodies used for IHC included anti-CS (Abcam, ab11570, at 1:400 dilution), anti-Phospho-Smad 2 (Abcam, ab188334, at 1:100 dilution), anti-Phospho-Smad 3 (Abcam, ab52903, at 1:100 dilution), anti-Sox 9 (Abcam, ab185230, at 1:400 dilution), anti-SCX (Biorbyt, orb306386, at 1:50 dilution), anti-Phospho-JNK (Santa Cruz, sc-12882, at 1:200 dilution), anti-Phospho-ERK (Santa Cruz, sc-23759-R, at 1:200 dilution), anti-Phospho-P38 (Abcam, ab4822, at 1:200 dilution).

Due to the relatively lower amount of HS in the AF and the lack of high-sensitivity anti-HS antibodies, we employed the more sensitive immunofluorescence (IF) approach, instead of chromogenic IHC, to visualize HS in the AF. For the IF analyses, the spines dissected from the 3-week-old control and cKO mice (3 mice from each group) were fixed overnight at 4 °C with 4% paraformaldehyde, and then decalcified in 0.1% DEPC-treated 15% EDTA solution at 4 °C for 7 days. Samples were dehydrated with 30% sucrose and embedded in OCT compound (Sakura Finetek Inc., Torrance, USA). Sections were cut at 5 μm on a cryostat (2800 FRIGOCUT; Leica). The sections were incubated at 37 °C for 1 h, rinsed in PBS and treated with 3% H_2O_2 to block endogenous peroxidase activity. After antigen retrieval treatment with hyaluronidase (SIGMA, H4272), the sections were incubated with 3% bovine serum albumin and 10% normal goat serum to block nonspecific reactions. Sections were then incubated with the anti-HS antibodies (Amsbio,

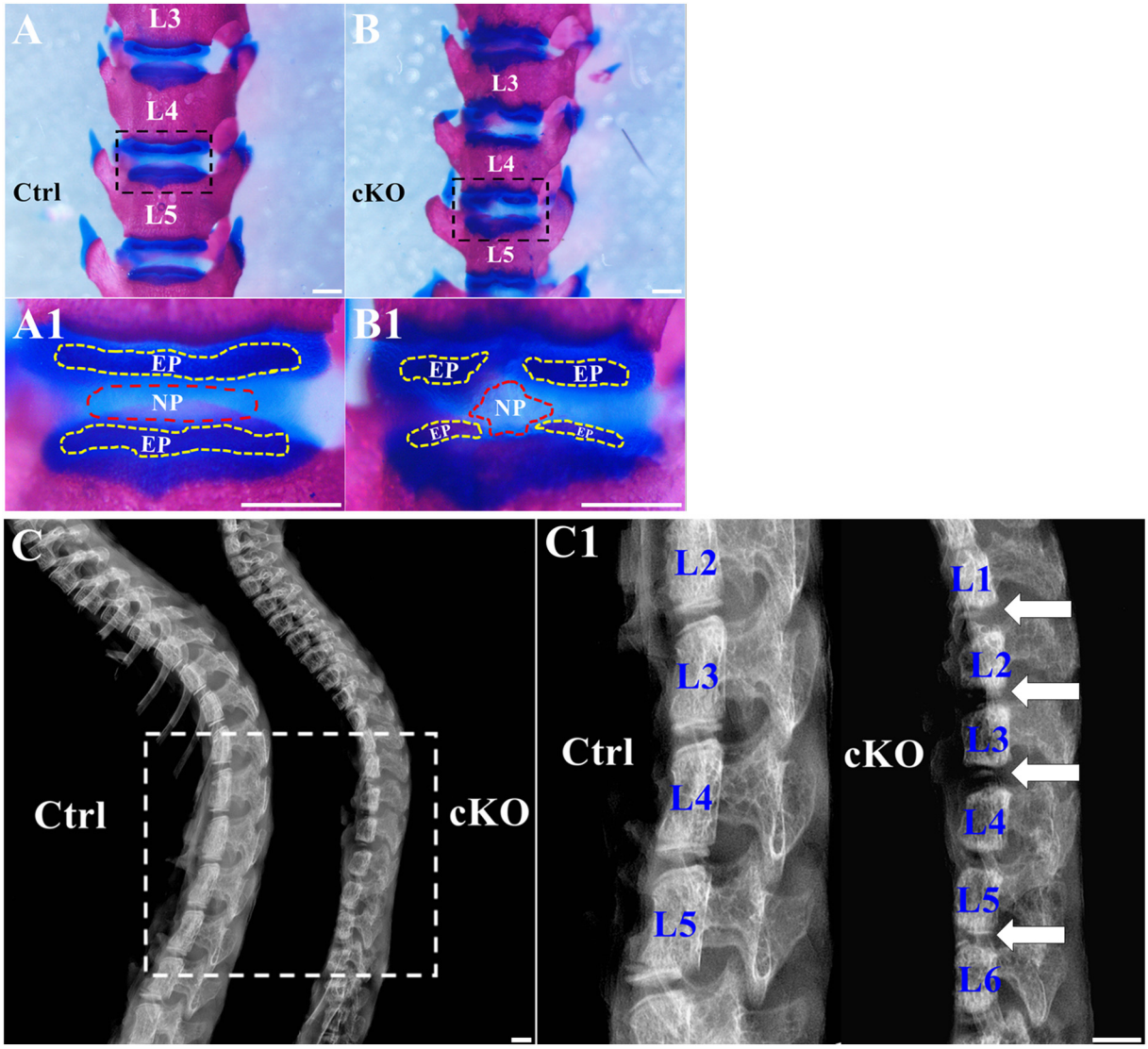

Fig. 3. Inactivation of FAM20B led to the shrinkage of NP and malformation of EP. (A, B) Alcian blue and alizarin red staining of the spines from 3-week-old control and cKO mice; the representative images (of at least 3 mice for each group) were the anterior views of the L3-L5 region of the spines. A1 and B1 were the higher magnification views of the black boxes in A and B, respectively. The size of NP (the area surrounded by red dashed lines) was reduced in cKO mice and the integrity of EP (the area surrounded by yellow dashed lines) was lost in cKO mice (Bars in the A, B, A1, B1 = 1 mm). (C) Plain X-ray images of the spines from 3-week-old control and cKO mice. C1 was the higher magnification view of white box in panel C. The white arrows indicated the malformed EP in cKO mice (Bars in the C, C1 = 1 mm).

clone F58-10E4, 370255-1, at 1:25 dilution) overnight at 4 °C. Next, sections were incubated with Goat Anti-Mouse IgM mu chain secondary antibodies (ab150121, at 1:200 dilution) at room temperature for 1 h. After washing with PBS, the slides were mounted with DAPI (Sigma, California, USA). SP5 Leica confocal microscope was used to capture the images. The positive signal for HS was in green; DAPI staining was in blue.

2.7. Western immunoblotting

Under stereo microscope (Nikon, MK II), the AF from the IVDs of 3-week-old cKO and normal control mice (3 mice from each group) were dissected. The AF tissues from each mouse were collected separately; i.e., the tissues from the 3 mice of each group were not pooled but were placed in 3 different containers and the proteins from the AF of each mouse were extracted independently. The dissected AF tissues were ground into powder in liquid nitrogen and lysed by RIPA buffer (ThermoFisher Scientific, NY, USA) supplemented with a mixture of protease inhibitors (Roche). Bicinchoninic Acid (BCA) assay (Pierce Biotechnology) was used to measure the protein concentrations of the samples for the normalization of sample loading sizes. The protein extracts from the AF of each mouse were independently analyzed by sodium dodecyl sulfate polyacrylamide gel electrophoresis (SDS-PAGE) and Western immunoblotting as we described previously [41]. We did multiple Western immunoblotting analyses on the protein extracts from the AF of each mouse. Primary antibodies used for Western immunoblotting were anti-Phospho-Smad 2 (Abcam, ab188334, at 1:1000 dilution), anti-Phospho-Smad 3 (Abcam, ab52903, at 1:1000 dilution), anti-Total-Smad 2/3 (Cell Signaling Technology, #8685, at 1:1000 dilution), anti-Sox 9 (Abcam, ab185230, at 1:1000 dilution), anti-SCX (Biorbyt, orb306386, at 1:500 dilution), anti-Phospho-JNK (Santa Cruz, sc-12882, 1:1000 at dilution), anti-Total-JNK (Abcam, ab179461, at 1:1000 dilution), anti-Phospho-ERK (Cell Signaling Technology, #9101, at 1:1000 dilution), anti-Total-ERK (Cell Signaling Technology, #4695, at 1:1000 dilution), anti-Phospho-P38 (Cell Signaling Technology, #4511, at 1:1000 dilution), and anti-Total-P38 (Cell Signaling Technology, #8690, at 1:1000 dilution). The goat-derived anti-rabbit IgG conjugated with horseradish peroxidase (sc-2030, Santa Cruz

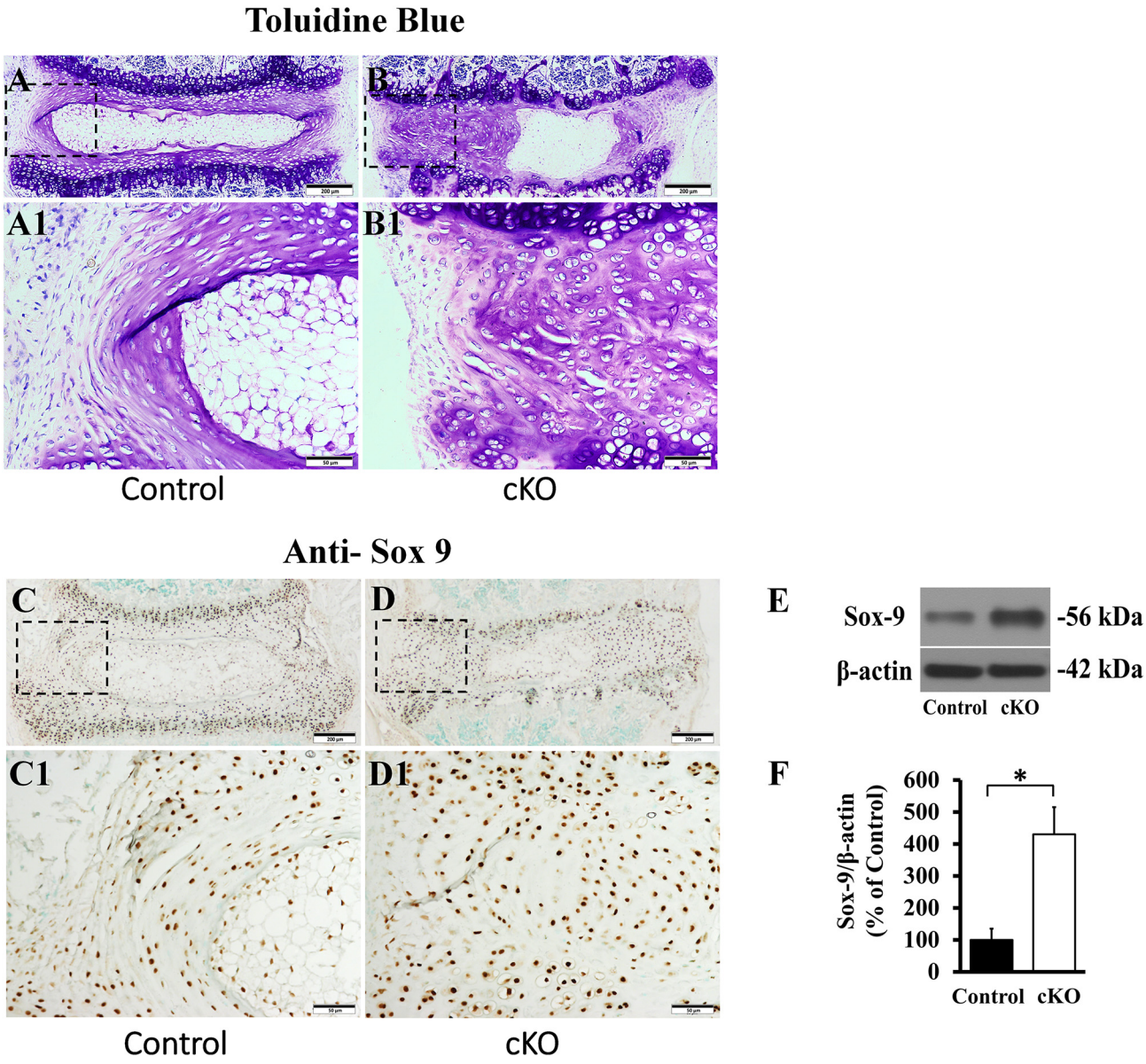

Fig. 4. Inactivation of FAM20B led to the formation of ectopic cartilage-like tissue in the outer AF. (A, B) Toluidine blue staining of IVDs in 3-week-old control and cKO mice (representative images of at least 3 mice for each group). A1 and B1 were the higher magnification views of the black boxes in A and B, respectively. The majority of AF in cKO mice was stained purple, while in the control mice, the toluidine blue dye was mainly located in the inner AF (Bars in the A, B = 200 μm, Bars in the A1, B1 = 50 μm). (C, D) IHC detection of Sox 9 in the IVD of 3-week-old control and cKO mice (representative images of at least 3 mice for each group, positive signals in brown). C1 and D1 were the higher magnification views of the black boxes in C and D, respectively. Note that the AF of cKO mice had more Sox 9-positive cells (Bars in the C, D = 200 μm, Bars in the C1, D1 = 50 μm). (E) Anti-Sox 9 Western immunoblotting of total proteins extracted from the AF of 3-week-old control and cKO mice. (F) The relative levels of Sox 9 protein as assessed by the protein band strengths in the Western immunoblotting analyses (n = 3, * = $P < 0.05$).

Biotechnology, Dallas, TX; 1: 2000) was used as the secondary antibody. The immunoreactive bands were detected with an enhanced chemiluminescence (ECL) detection system (Pierce Biotechnology), according to the manufacturer's instructions, and the signals were visualized with CL-XPosure film (Pierce Biotechnology Inc., Rockford, Ill., USA). The chemiluminescence protein bands of interest were assessed using the NIH Image J software (National Institutes of Health, Bethesda, MD, USA) to measure the overall signal strength, which integrated the area and intensity of a protein band; if a protein appeared as doublet bands, both bands were assessed. Western immunoblotting was performed independently on the protein extracts from each of the 6 mice (3 from each group) and same conditions were applied to the immunoblotting processes for assessing the same protein. The average signal strength of each target protein was calculated from 3 independent assessments for each group and the value was expressed as the signal strength of the individual protein in relativity (ratio) to that of β-actin in the quantitative analyses.

2.8. RNA isolation and quantitative real-time PCR (QRT-PCR) analysis

Under stereo microscope (Nikon, MK II), the AF from the IVDs of 3-week-old cKO and normal control mice (6 mice from each group) were dissected. As in the Western immunoblotting analyses, we collected the AF tissues from each mouse separately and used RNeasy mini Kit (Qiagen, Inc., Valencia, CA) to extract total RNA independently (without pooling) from the samples of each mouse. The extracted total RNA was treated with DNase I (Promega, Madison, WI) to remove genomic DNA. The RNA purity and concentration were assessed with a NanoDrop spectrophotometer (DeNovix, DS-11 +). The integrity of RNA was verified on ethidium bromide stained agarose gels. The RNA

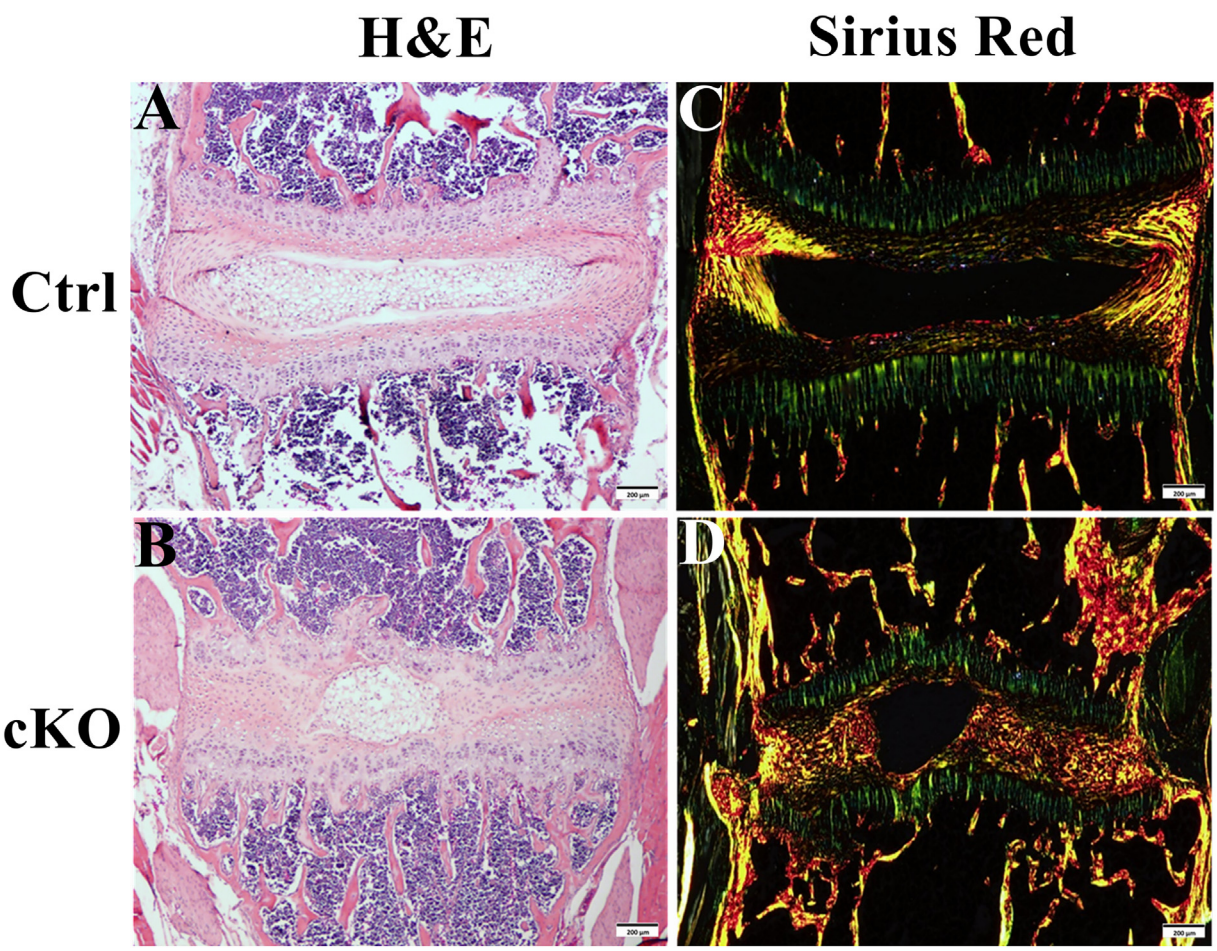

Fig. 5. Inactivation of FAM20B caused collagen structure changes in AF. (A, B) H&E staining of IVD from 3-week-old control and cKO mice (Bars in the A, B = 200 μm). (C, D) Sirius red staining of IVD in 3-week-old control and cKO mice (Bars in the C, D = 200 μm). A–D was the representative images of at least 3 mice for each group. Note the severe disruption of the collagen structure and thinner and more irregular fibers in the AF of cKO mice. Also note the loss of lamellae in AF of cKO mice.

(1 μg/ml per sample) was transcribed into cDNA using QuantiTect Reverse Transcription Kit (Qiagen) according to the protocol provided by the manufacturer. Then, GoTaq® qPCR Master Mix (Promega) was used for SYBR green real-time RT-PCR technique to assess the mRNA levels of Col I, Col II and SCX. Samples, in which no reverse transcriptase was added, were set as the negative control. Glyceraldehyde 3-phosphate dehydrogenase (GAPDH) was used as a housekeeping gene and all the samples were normalized to the GAPDH level and fold changes were calculated by relative quantification ($2-\triangle\triangle Ct$). The experiments for each group were performed with six biological replicates. The primers used for the amplification of the indicated genes were listed as below: Col I (Forward) CTGCTGGCAAAGATGGAGA, (Reverse) ACCAGGAAGACCCTGGAATC [42]; Col II (Forward) GGAA AGTCTGGGGAAAGAGG, (Reverse) CAGTCCCTGGGTTACCAGAA [43]; SCX (Forward) CCTTCTGCCTCAGCAACCAG, (Reverse) GGTCCAAAGT GGGGCTCTCCGTGACT [44]; GAPDH (Forward) CAAAGTTGTCATGG ATGACC, (Reverse) CCATGGAGAAGGCTGGGG [45];

2.9. In situ hybridization (ISH)

ISH was performed on the paraffin sections made of the spine specimens from 3-week-old mice. The RNA probes for Col I and Col II were the same as we used in our previous studies [22]. The probes were labeled with digoxigenin (DIG) using a RNA labeling kit (Roche Life Science, IN, USA), according to the manufacturer's instructions. Anti-DIG-AP antibody (Roche Life Science) and alkaline phosphatase chromogen (BCIP/NBT) substrate (Vector Laboratories) were used to detect the DIG-labeled RNA probes. The positive signals were stained blue.

2.10. Statistical analysis

All quantitative data were analyzed by SPSS 13.0 software and presented as mean ± SD from 3 to 6 biological independent experiments. All data were tested for and confirmed to present normal distribution using Shapiro-Wilk test. The Student's *t*-test was used to compare the means between two groups. A value of $p < 0.05$ was considered statistically significant.

3. Results

3.1. Inactivation of FAM20B causes growth retardation and spine deformity

By crossbreeding the *Fam20B*$^{flox/flox}$ mice with the transgenic mice expressing *Cre*-recombinase driven by the *2.3kb Col 1a1* promoter, we generated the *2.3kb Col 1a1-Cre;Fam20B*$^{flox/flox}$ mice (referred to as "cKO mice" in this report), in which FAM20B was inactivated in the cells expressing Type I collagen. We characterized cKO mice, in comparison with the *Fam20B*$^{flox/flox}$ littermates that served as normal controls (Ctrl). The cKO mice showed apparent postnatal growth retardation compared to the age- and gender-matched normal controls (Fig. 1). At birth, the body mass of cKO mice was similar to that of the normal

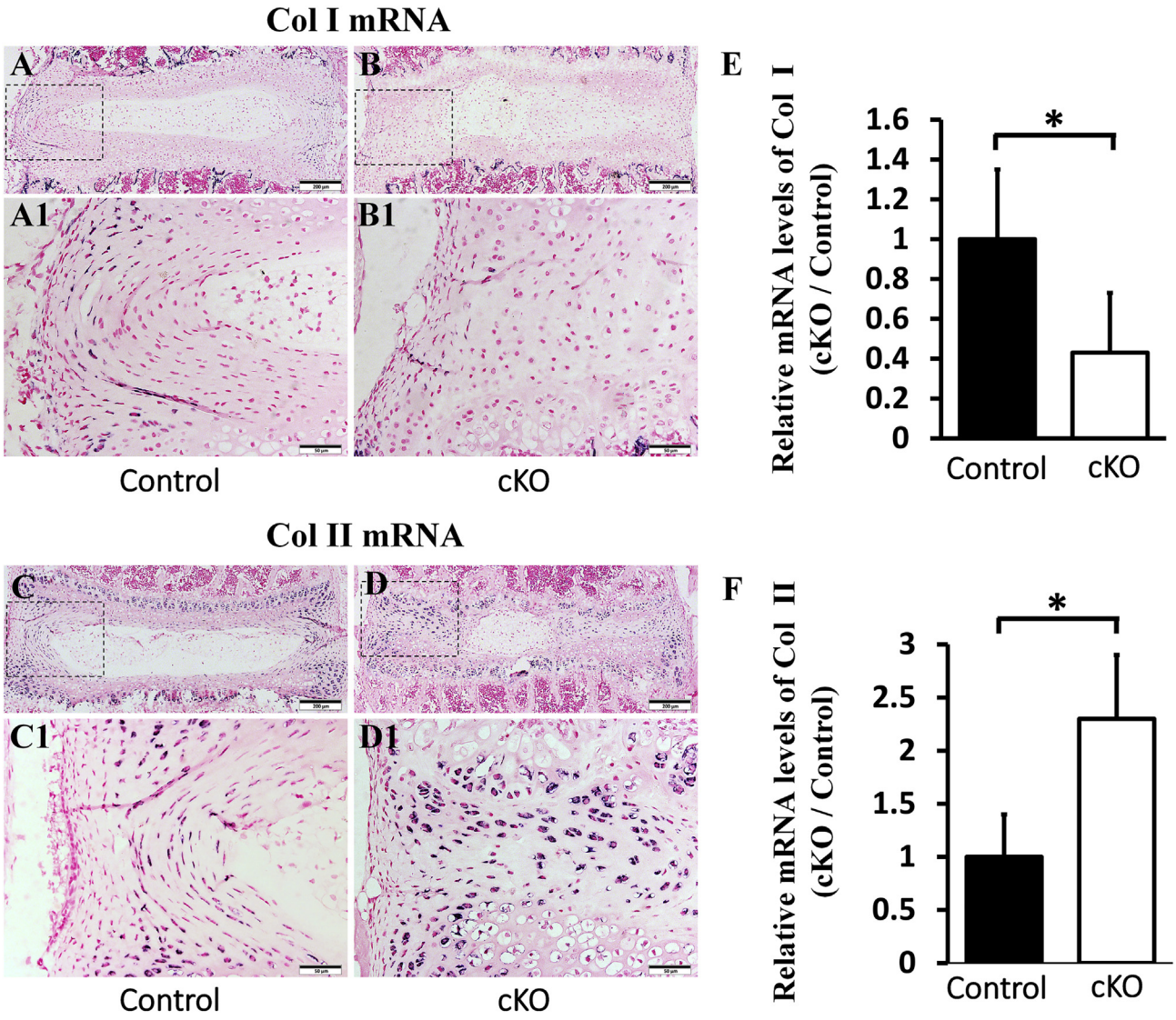

Fig. 6. Inactivation of FAM20B altered the collagen composition of AF. (A, B) In situ hybridization analyses of Col I mRNA in the IVD of 3-week-old control and cKO mice. A1 and B1 were the higher magnification views of the black boxes in A and B, respectively (Bars in the A, B = 200 μm, Bars in the A1, B1 = 50 μm). (C, D) In situ hybridization analyses of Col II mRNA in the IVD of 3-week-old control and cKO mice. C1 and D1 were the higher magnification views of the black boxes in C and D, respectively (Bars in the C, D = 200 μm, Bars in the C1, D1 = 50 μm). A–D was the representative images of at least 3 mice for each group. (E, F) QRT-PCR analyses of Col I and Col II mRNA in 3-week-old mice showed that the Col I mRNA level was significantly lower and Col II level was much higher in the AF of cKO mice than in the control mice (n = 6, * = $p < 0.05$).

control mice, and at postnatal two weeks, the body mass in cKO mice became significantly lower than in the normal controls. As the mice further aged, the difference in body weight became more prominent. At postnatal three weeks, body mass of cKO mice was approximately 70% of the normal ones (Fig. 1B). At postnatal 12 weeks, the body mass of cKO mice was approximately 50% of the normal controls (Fig. 1B). X-ray radiographic examinations showed that the tails and the spines of cKO mice were remarkably shorter than those of the controls and the curvature of spine in cKO mice was changed showing severe kyphosis (Fig. 1C).

3.2. Inactivation of FAM20B causes abnormalities in IVD

For morphological analyses, we first performed H&E staining to assess the effects of FAM20B inactivation on the development of mouse IVD. In the IVD from 3-week-old mice, the sagittal sections (sections created by cutting the IVD in a front-back direction) revealed mild-moderate abnormalities in EP and NP, with the EP being thinner and the NP becoming smaller; the anterior and posterior AF of cKO mice appeared slightly different from the controls in the sagittal sections (Fig. S1).

In the coronal sections (i.e., sectioning the IVD in a left-right direction), cKO mice at E 16.5 and at birth showed mildly malformed IVD, with the AF cells becoming larger and rounder, compared to the AF cells in the normal controls (Fig. 2A, B, C, D). At postnatal 1 and 3 weeks, the IVD of cKO mice demonstrated remarkable deformities and the phenotypic differences of IVD became much more apparent between cKO and control mice (Fig. 2E, F, G, H,I). From postnatal 1 week, the outer AF cells in cKO mice started to exhibit morphological change; unlike the fibroblast-like cells observed in the outer AF of control mice, the outer AF cells in cKO mice became rounder and took a chondrocyte-like appearance. Due to the morphological change of the outer AF cells, the boundary between the inner AF and the outer AF became less clear. This morphological alteration of the outer AF cells became more apparent in the cKO mice at postnatal 3 weeks at which point the entire outer AF was replaced by disorganized chondrocytes. Additionally, the

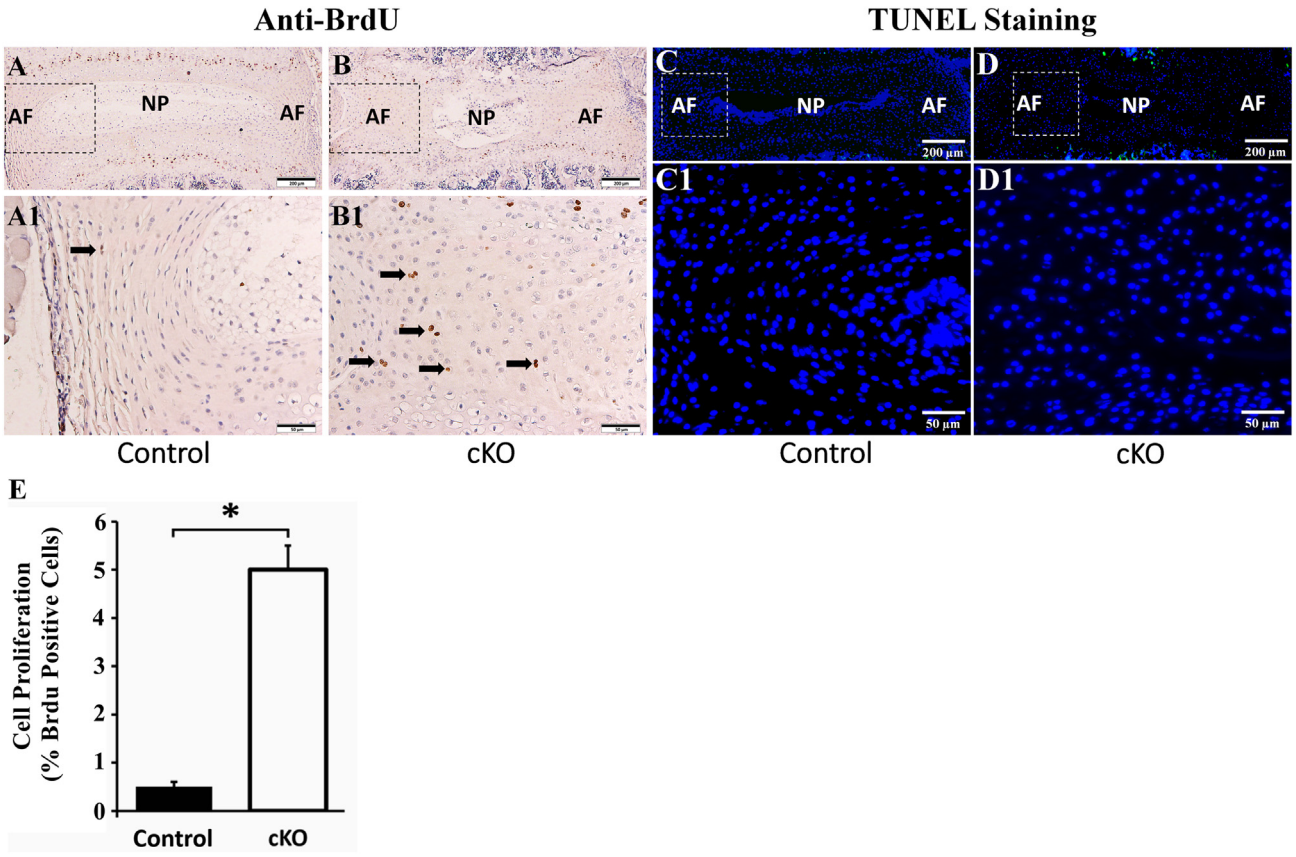

Fig. 7. Inactivation of FAM20B increased the proliferation of AF cells. (A, B) Anti-BrdU staining of IVDs in 3-week-old control and cKO mice (representative images of 6 mice from each group). A1 and B1 were the higher magnification views of the black boxes in A and B, respectively. The number of BrdU-positive AF cells (indicated by black arrows) in cKO mice was greater than in the control mice (Bars in the A, B = 200 μm, Bars in the A1, B1 = 50 μm). (C, D) TUNEL staining of IVDs in 3-week-old control and cKO mice (representative images of 3 mice from each group). C1 and D1 were the higher magnification views of the white boxes in C and D, respectively. No apoptosis cells were found in the AF of control and cKO mice while positive signals of TUNEL (green) were observed in the growth plates of these mice (Bars in the C, D = 200 μm, Bars in the C1, D1 = 50 μm). (E) Quantitative comparison of cell proliferation rates between AF cells of cKO mice versus the control mice as measured by the BrdU-positive cells. (n = 6; * = $p < 0.05$).

NP of 1- and 3-week-old cKO mice showed dramatic shrinkage in size, allowing the majority areas of IVD being replaced by the malformed AF. EP deformities were also obvious in the coronal sections; the average EP heights in 1- and 3-week-old control mice were 85.2 ± 4.5 μm and 65.7 ± 5.7 μm, respectively, while those of cKO mice were 27.3 ± 4.3 μm and 8.5 ± 7.6 μm, respectively. In some areas of IVD in the 3-week-old cKO mice, EP was even lost, which allowed the NP to invade into the adjacent growth plate. It was apparent that the functional loss of FAM20B had more significant effects on the development of the lateral parts of the IVD than on the anterior and posterior regions. In the following sections, we will use the coronal sections of IVD tissues to illustrate our findings in the lateral parts of the IVD.

We stained the spines of 3-week-old mice with alcian blue and alizarin red; in this assessment, chondrocytes and cartilage-like tissues are stained blue, while bone and mineralized tissues stained red. The area of NP was significantly smaller and the integrity of EP was lost (Fig. 3A, B) in cKO mice. X-ray radiographic analyses of the spines showed severely malformed EP in cKO mice (Fig. 3C, C1). These observations further confirmed the results of H&E staining that inactivation of FAM20B disrupted the development of IVD.

No significant phenotypic differences in IVDs were observed between the male and female cKO mice in any of the above described analyses.

3.3. Inactivation of FAM20B led to the formation of ectopic cartilage-like tissue in the outer AF

AF is a fibrocartilage structure located around the NP. AF is subdivided into inner AF and outer AF. Under physiological conditions, the inner AF cells are round, resembling chondrocytes, while the outer AF cells have a spindle-shaped morphology looking like fibroblasts [46]. As shown in Fig. S2, type I-expressing cells in this embryonic stage were mainly located in AF but not in NP and EP, consistent with our observation that the most remarkable abnormalities in the IVD of cKO mice were the phenotypic changes of AF that expressed the *2.3 kb Col 1a1-Cre* recombinase [38,39]. In the following section, we will describe and discuss in details of our findings about the malformed AF in cKO mice.

Toluidine blue staining, in which cartilaginous tissues are stained purple, revealed that in the control mice the toluidine blue was primarily restricted to the inner AF, while in the cKO mice, most of the AF areas including a major portion of the presumptive outer AF in cKO mice was stained purple, indicating that the fibrous tissues in the outer AF of the cKO mice was replaced by cartilage-like tissue (Fig. 4A, B). The IHC analyses for Sox 9, a specific marker of chondrocyte [47], revealed that the AF tissue in cKO mice had more Sox 9-positive cells than in the control mice. The Sox 9-positive cells were distributed across the whole AF in the cKO mice, while in the AF of control mice the Sox 9-positive cells were mainly located in the inner AF (Fig. 4C, D). Western immunoblotting analyses of total proteins extracted from the dissected AF tissue of IVD further confirmed the elevation of Sox 9

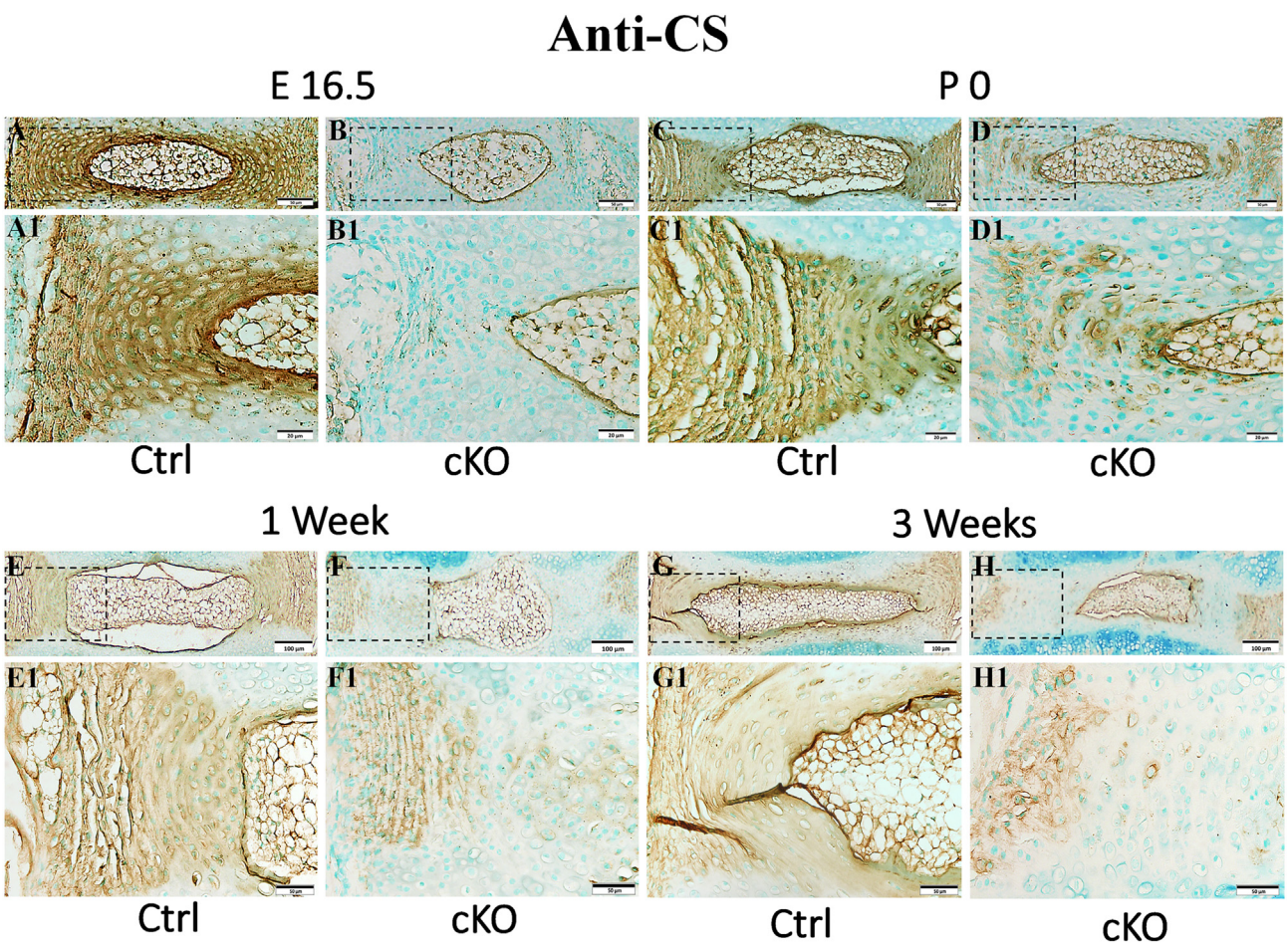

Fig. 8. Inactivation of FAM20B caused a reduction of chondroitin sulfate (CS) in AF. IHC detection of CS in the IVDs of E16.5 (A, B), P0 (C, D), 1-week-old (E, F) and 3-week-old (G, H) control and cKO mice (representative images from at least 3 mice for each group at each time point). A1, B1, C1, D1, E1, F1, G1 and H1 were the higher magnification views of the black boxes in A, B, C, D, E, F, G and H respectively (Bars in the A, B, C, D, E1, F1, G1, H1 = 50 μm, Bars in the A1, B1, C1, D1 = 20 μm, Bars in the E, F, G, H = 100 μm). Note the reduction of CS in the IVDs of cKO mice. CS was even completely lost in some areas of AF in cKO mice.

protein in the AF of the cKO mice (Fig. 4E, F).

As cartilaginous change is usually associated with alterations in collagen structure, we analyzed the collagen fibers in AF by sirius red staining. The AF in cKO mice displayed a severe disruption of the collagen structure; the collagen fibers in the AF of cKO mice became thinner and more irregular, along with a total loss of the normal AF lamellae, the thin plate-like collagen structure, which is present in the normal control mice (Fig. 5C, D).

Our in situ hybridization (ISH) analyses showed that in the normal control mice, cells positive for Col I transcripts were mainly located in the outer AF while Col II-positive cells were predominantly present in the inner AF (Fig. 6). In cKO mice, the Col I-positive cells in the periphery of the AF were fewer than in the normal controls. On the contrary, the number of Col II-positive cells was significantly increased and distributed nearly across the entire AF in the cKO mice. Quantitative real-time PCR (QRT-PCR) analyses revealed a remarkable elevation of Col II mRNA (235% of control) and a significant reduction of Col I mRNA (43% of control) in the AF of cKO mice (Fig. 6E, F). Taken together, these results indicate that the outer AF in the cKO mice was transformed from fibrous tissue to cartilage-like tissue.

As the AF in cKO mice was thicker than that of the control mice (Fig. 2), we suspected that the proliferation rate of AF cells might have been elevated. To determine the proliferation rate of the AF cells, we performed intraperitoneal injection of BrdU in the mice. Antibodies against BrdU were used to detect the proliferating cells that were actively replicating their DNA [35]. As shown in Fig. 7A, B, E, the AF in the cKO mice had more (approximately 9.5 folds over the control group) BrdU-positive cells than in the control mice. However, TUNEL staining analyses showed that there was no significant apoptosis in the AF cells of either control or cKO mice (Fig. 7C, D).

3.4. Inactivation of FAM20B caused a reduction of chondroitin sulfate in AF

FAM20B is a xylose kinase that catalyzes the assembly of CS, the most abundant GAG in the AF tissue and critical for the development and maintenance of AF [16]. Our anti-CS IHC analyses revealed that the AF of IVD in cKO mice had remarkably less CS than in the control mice (Fig. 8). In some areas of the AF of cKO mice, CS was even completely lost. The NP in cKO mice also had less CS than in control mice although the quantitative change of CS in the NP was not as dramatic as that in the AF. Immunofluorescence analyses showed that the AF of cKO mice also had less HS than that of the normal control mice (Fig. S3).

3.5. The functional loss of FAM20B in AF altered the levels of molecules in the TGFβ signaling pathway

TGFβ signaling pathway is known to be essential for the development and maintenance of AF in IVD [24–26]. The activation of TGFβ signaling pathway depends on the phosphorylation of Smad 2 and Smad 3. The phosphorylated forms of Smad 2 and Smad 3 bind to Smad4 to form a complex, which then enters the nucleus to activate the

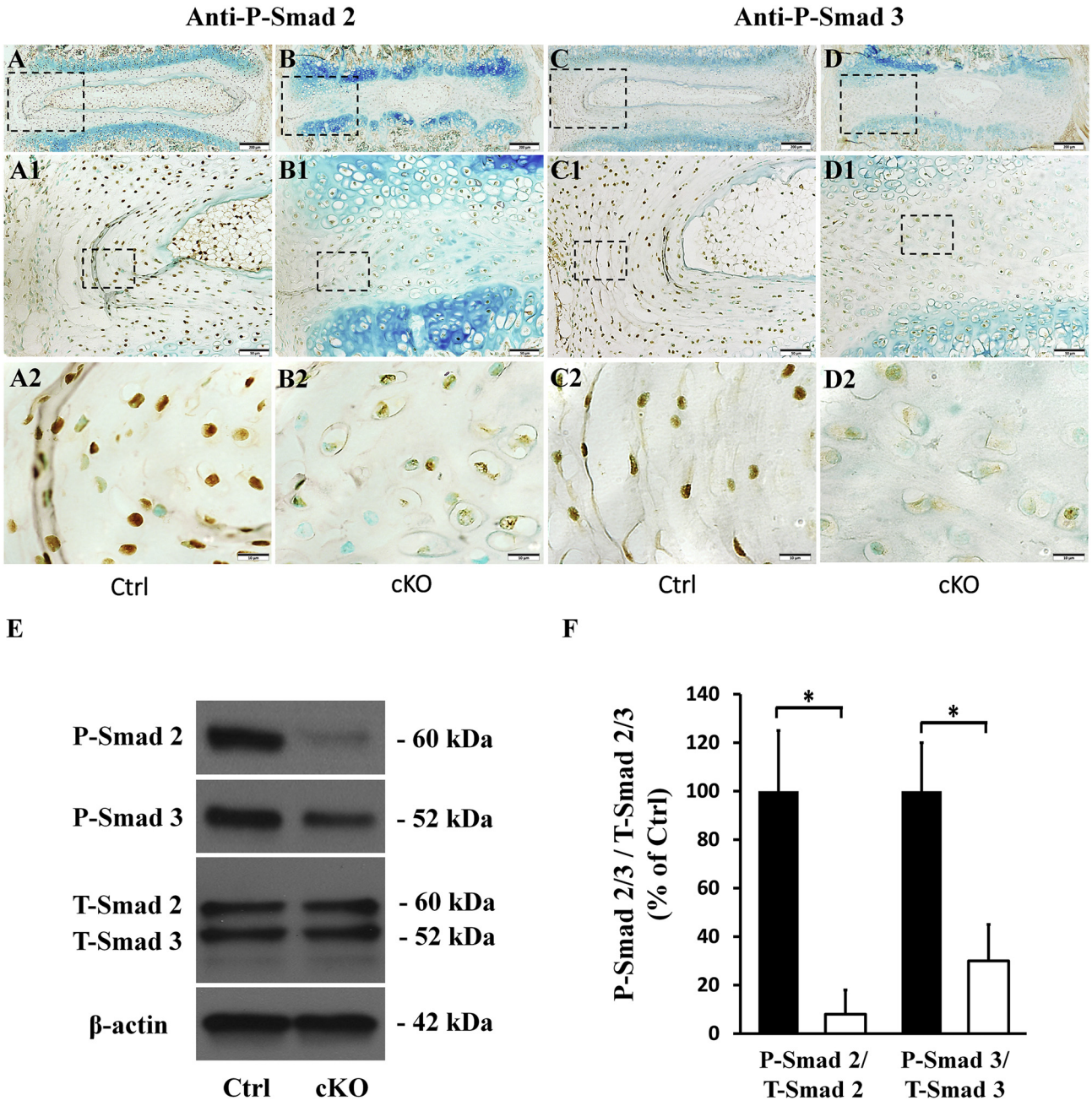

Fig. 9. Inactivation of FAM20B inhibited the activation of TGFβ signaling pathway in AF. (A, B, C, D) IHC Detection of P-Smad 2 and P-Smad 3 in IVDs of 3-week-old control and cKO mice (representative images of at least 3 mice for each group). A1, B1, C1, D1 were the higher magnification views of the black boxes in A, B, C, D, respectively. A2, B2, C2, D2 were the higher magnification views of the black boxes in A1, B1, C1, D1, respectively. The numbers of P-Smad 2 or P-Smad 3 positive cells were reduced in the AF of cKO mice (Bars in the A, B, C, D = 200 μm, Bars in the A1, B1, C1, D1 = 50 μm, Bars in the A2, B2, C2, D2 = 10 μm). (E) Protein levels of P-Smad 2 and P-Smad 3 in AF as revealed by Western immunoblotting. (F) Relative levels of P-Smad 2 and P-Smad 3 to total P-Smad 2/3 determined by Western immunoblotting (n = 3; * = $p < 0.05$). The protein levels of both P-Smad 2 and P-Smad 3 were significantly lower in the AF of cKO mice. For Western immunoblotting analyses, the total proteins were extracted from AF of 3-week-old control and cKO mice.

transcriptions of target genes [48]. In this study, we examined the levels of phospho-Smad 2 and phospho-Smad 3 in the AF of the control and cKO mice by immunohistochemistry and Western immunoblotting analyses. As shown in Fig. 9, the numbers of cells positive for phospho-Smad 2 and phospho-Smad 3 were much fewer in the AF of cKO mice than in the control mice. Western immunoblotting analyses of total proteins extracted from the AF revealed that the levels of phospho-Smad 2 and phospho-Smad 3 were significantly lowered in the AF of cKO mice, with those of total Smad 2 (T-Samd 2) and Smad 3 (T-Smad 3) unchanged; the ratio of phospho-Smad 2 to T-Smad 2 in cKO mice was 8.1% of the control mice and the that of phospho-Smad 3 to T-Smad 3 in cKO mice was 30.7% of the control. These results indicate that in the AF of cKO mice the activation of Smad-dependent TGFβ signaling pathway may be inhibited.

Scleraxis (SCX), an AF marker, is a downstream target molecule of TGFβ signaling pathway [49]. IHC analyses showed that the number of SCX-positive cells was lower in the AF of cKO mice than in the control mice (Fig. 10). Anti-SCX Western immunoblotting analyses of proteins extracted from the AF confirmed that the AF of cKO mice had reduced level of SCX protein (43.8% of control). Additionally, we extracted the total RNAs from AF and observed that the AF of cKO mice showed a reduced SCX mRNA level (32.5% of control).

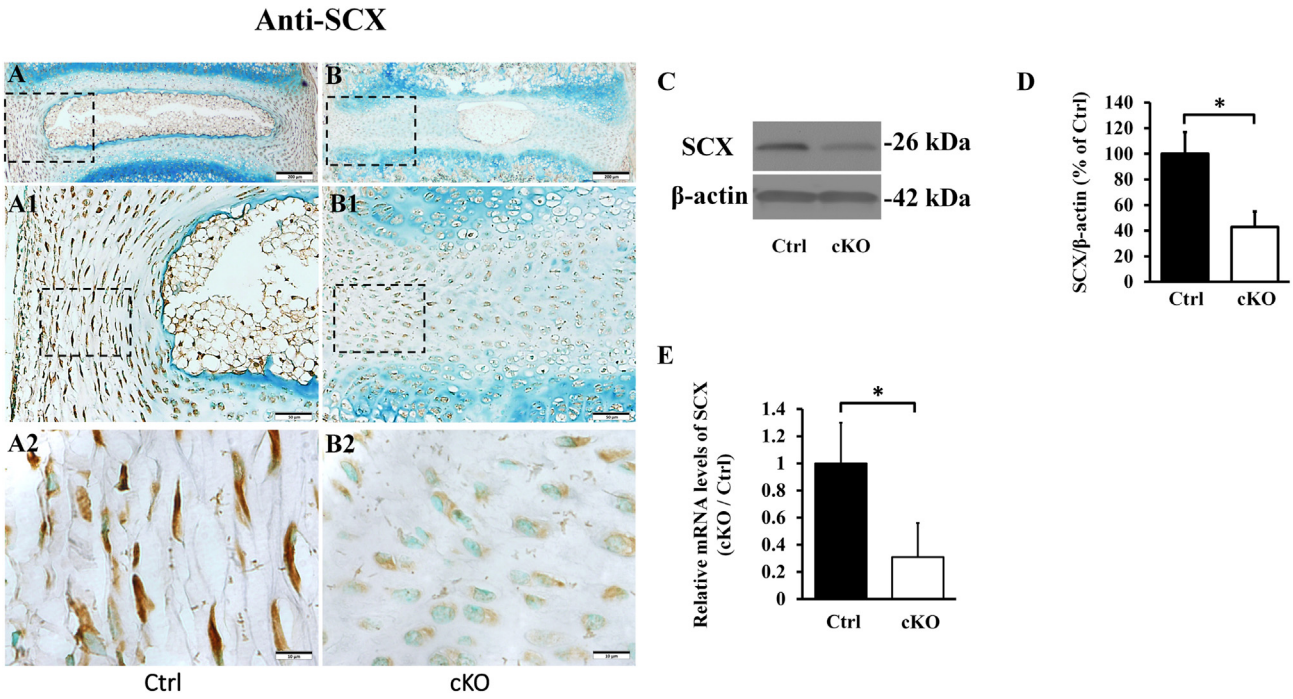

Fig. 10. Inactivation of Fam20B reduced the expression of SCX in AF. (A, B) IHC detection of SCX in the IVD of 3-week-old control and cKO mice (representative images of at least 3 mice for each group). A1 and B1 were the higher magnification views of the black boxes in A and B, respectively. A2 and B2 were the higher magnification views of the black boxes in A1 and B1, respectively (Bars in the A, B = 200 μm, Bars in the A1, B1 = 50 μm, Bars in the A2, B2 = 10 μm). Note the reduced number of SCX-positive cells in the AF of cKO mice. (C) Anti-SCX Western immunoblotting. (D) Relative levels of SCX protein illustrated in Western immunoblotting analyses (n = 3, * = $p < 0.05$). The protein level of SCX was markedly lower in AF of cKO mice than in the control. The total proteins were extracted from the AF of 3-week-old mice. (E) SCX mRNA levels detected by QRT-PCR analyses of total mRNAs extracted from the AF of 3-week-old mice; note the reduced level of SCX mRNA level in the AF of cKO mice (n = 6, * = $p < 0.05$).

3.6. The functional loss of FAM20B in AF altered the levels of molecules in the MAPK signaling pathways

MAPK signaling pathways includes MAPK-JNK, MAPK-ERK and MAPK-P38 pathways. The activation of MAPK signaling pathways are mediated via the phosphorylation of JNK, ERK and P38 by their corresponding kinases [50]. To study whether ablation of FAM20B also had effects on the activation of MAPK signaling pathways, we examined the levels of phospho-JNK, phospho-ERK and phospho-P38 in the AF of control and cKO mice by immunohistochemistry (IHC) and Western immunoblotting. IHC analyses showed that compared to the control mice, the AF of cKO mice contained fewer phospho-JNK-positive cells, and had more phospho-ERK- and phospho-P38-positive cells (Fig. 11), Western immunoblotting analyses of proteins extracted from the AF confirmed that the level of phospho-JNK was lower and those of phospho-P38 and phospho-ERK were higher in the AF of cKO mice than in the control mice, while the levels of total JNK, total P38 and total ERK were similar between the cKO and control mice (Fig. 11). The ratio of phospho-JNK to T-JNK in cKO mice was 7.5% of control mice, while the ratio of phospho-P38 to T-P38 and that of phospho-ERK to T-ERK in cKO mice were 621.5% and 1211.2% of the control, respectively (The uncropped bands of western immunoblotting were shown in Fig. S4).

4. Discussion

Studies have shown that the constitutive ablation of *Fam20B* in mice results in embryonic lethality and that the functional loss of the FAM20B in zebrafish causes aberrant cartilage formation and severe skeletal defects, which are linked to abnormal proteoglycan (PG) biosynthesis [35]. In this study, we inactivated FAM20B in the type I collagen-expressing cells by mating the *Fam20B*-floxed mice with the transgenic mice expressing a transgenic Cre-recombinase driven by the *2.3 Col I* promoter. We observed a dramatic growth retardation in these *Fam20B* conditional knockout (cKO) mice. After postnatal 2 weeks, the body weight of cKO mice was significantly smaller than the control mice and the spines of the cKO mice were obviously malformed with remarkably shorter spine and severe kyphosis. In particular, the IVD of cKO mice showed defects. These results have confirmed the critical role of FAM20B in spine development.

In the vertebrates, proper development and maintenance of IVD are essential to the structural integrity of spine, and a normal structure of spine ensures the appropriate functions of this organ, which include bearing the body weight and supporting movements. The three components of IVD, nucleus pulposus (NP), endplates (EP) and annulus fibrosus (AF) are interdependent to one another in structure and function in exerting the physiological functions of the IVD and spine.

In cKO mice, both the NP and EP were defective; NP was smaller than that in the normal mice and the integrity of EP was lost. It is reported that the excessive mechanical loading of IVD will destroy the normal functions and structures of IVD [51,52]. The defective changes of NP and EP in our study were probably attributed to the abnormal mechanical stress distribution of IVD associated with the structural and functional deficiency of AF due to the inactivation of FAM20B in AF that expresses type I collagen and in which the cre-recombinase was active in cKO mice. The matrix synthesis of the disc cells are closely related to the mechanical stress and acute mechanical injury or accumulated overloading could inhibit disc cell metabolism and accelerate matrix degradation of IVD [53,54]. In this study, the abnormal distributions of disc stress caused by malformed AF might reduce the metabolism of disc cell and accelerate matrix degradation of NP and EP, which may have collectively caused the severe malformation of entire IVD in cKO mice.

AF derives from sclerotome [55]. The developing AF is further differentiated into inner AF and outer AF. Inner AF is fibrocartilage that exhibits characteristics of both fibrous tissues and cartilaginous tissue while outer AF is more fibrous and resembles ligament and tendon [56].

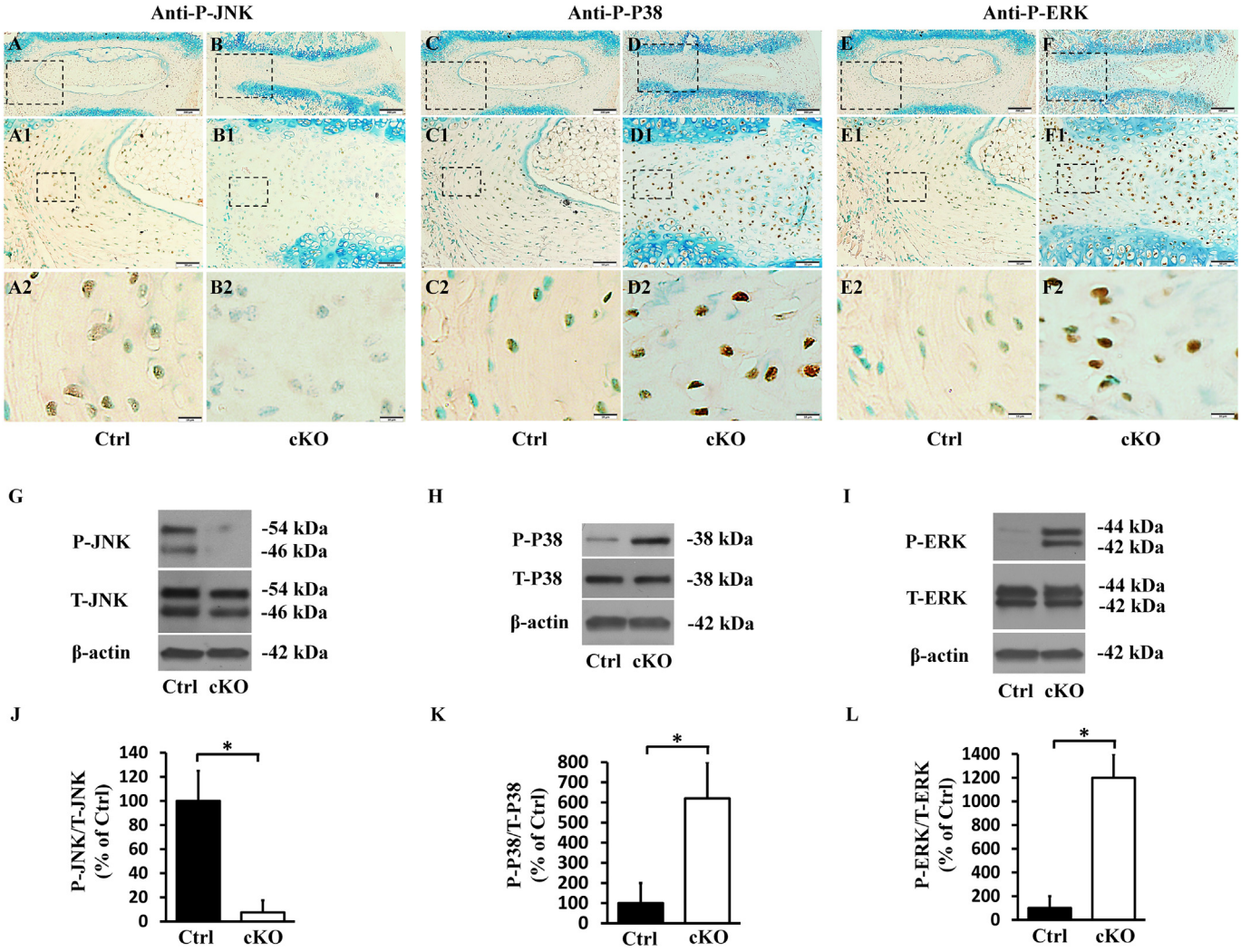

Fig. 11. Inactivation of FAM20B altered the levels of molecules in MAPK signaling pathway in AF. (A, B, C, D, E, F) IHC analyses of P-JNK, P—P38 and P-ERK in the IVDs of 3-week-old control and cKO mice (representative images of at least 3 mice for each group). A1, B1, C1, D1, E1, F1 were the higher magnification views of the black boxes in A, B, C, D, E, F, respectively. A2, B2, C2, D2, E2, F2 were the higher magnification views of the black boxes in A1, B1, C1, D1, E1, F1, respectively. The numbers of P-JNK positive cells were reduced in the AF of cKO mice, while the numbers of P—P38 and P-ERK positive cells were significantly increased in the AF of cKO mice (Bars in the A, B, C, D, E, F = 200 μm, Bars in the A1, B1, C1, D1, E1, F1 = 50 μm, Bars in the A2, B2, C2, D2, E2, F2 = 10 μm). (G, H, I) Protein levels of P-JNK, P—P38 and P-ERK in the AF of 3-week-old mice as detected by Western immunoblotting. (J, K, L) Relative levels of P-JNK, P—P38 and P-ERK to total JNK, P38 and ERK illustrated in Western immunoblotting analyses. The protein level of P-JNK was lower while those of P—P38 and P-ERK were significantly higher in AF of cKO mice than in the control ($n = 3$, * = $p < 0.05$).

Traumatic injuries or developmental defects of AF are major causes of IVD herniation in humans, leading to serious clinical symptoms, such as lower back pain, leg pain and disability, which severely affect the patients' quality of life [57]. The normal structure and function of AF is closely related to the integrity of ECM. A decrease in ECM content or the component alteration may affect the structure of AF and cause loss of its function [11,12]. GAGs, as a major component of ECM of AF, play an important role in the development of AF [14,16,58]. Therefore, FAM20B, as an enzyme essential for the synthesis of GAGs, may play an important role in the normal development of AF.

In this study, we inactivated FAM20B in the type I-expressing cells. While in the embryonic stage, the type I-expressing cells distribute throughout the entire AF with higher number in the outer AF and relatively lower number in the inner AF. Our in situ hybridization analyses did not show the presence of type I collagen-expressing cells in the NP and EP; indicating that in the IVD of cKO mice FAM20B was inactivated in the AF, but may not be in NP and EP. We observed that the cells in the AF of cKO mice lost their normal spindle-shape, and became rounder and enlarged resembling chondrocytes. The findings of altered proteoglycan distribution detected by toluidine blue staining and increased expression of Sox 9, along with the morphologic change indicate that the cells of outer AF in the IVD of cKO mice have undergone a cell fate change; they were transformed from fibroblast-like cells to chondrocyte-like cells. The cell proliferation rate of AF cells in cKO mice was markedly higher than that of control mice. The increased proliferating cells in AF occupied the position of NP, which might have hastened the shrinkage of NP tissues and accelerated the destruction of IVD in cKO mice.

ECM components play an important role in the differentiation of AF cells [59]. The ECM of AF is mainly comprised of GAG-rich proteoglycans including Aggrecan, Versican, Decorin, Biglycan and Fibromodulin [15,60] and collagen fibers primarily consisting of type I and type II collagens. FAM20B is a xylose kinase essential to the elongation of CS and HS chains. CS is the most abundant GAG located in AF [16]. In young human AF tissue, CS accounts for 90% of total GAGs while the content of HS is below 2% [58]. In this study, we observed reduced levels and/or altered distribution of CS and HS in the AF of cKO mice, suggesting that loss of FAM20B affected the biosynthesis and

distribution of CS and HS in AF. The strong staining of toluidine blue in some areas of the outer AF in cKO mice may be attributed to the fact that the majority of the outer layer of AF was transformed from fibrous tissue to cartilaginous tissue; the latter synthesizes much more GAGs than the former. Another reason for the increased staining of toluidine blue may be that the deletion of FAM20B cannot abolish all kinds of GAG chains [35]; in addition to CS and HS, cartilage also contains keratin sulfate (KS) and hyaluronic acid (HA) [60], the synthesis of which does not need FAM20B. It is possible that the reduction of CS was compensated to a certain extent by the production of GAGs such as KS and HA, which do not need the catalysis by FAM20B. Sirius red staining revealed a dramatic disorganization of the collagen fibers while in situ hybridization and QRT-PCR revealed a decreased level of Col I mRNA and an increase of Col II mRNA in the AF of cKO mice. A reduction of Type I collagen, a marker of fibroblasts in AF, may weaken the tensile of disc and make the AF tissue not strong enough to sustain the expansion pressure from NP. This may eventually lead to the collapse of IVD tissue. The increased expression of type II collagen, a marker of chondrocyte, together with the results of enhanced toluidine blue staining and increased Sox 9 expression, suggests that the inactivation of FAM20B leads to cell fate changes in AF tissue with the outer AF cells undergoing a transformation from fibroblast-like cells to cartilaginous cells.

TGF-β signaling pathway is involved in the development and morphogenesis of many tissues. It is reported that TGF-β signaling participates in the development of AF. Sohn et al. demonstrated that TGF-β signaling pathway regulates the differentiation of AF cells and prevents chondrocyte differentiation in the presumptive AF tissue [61]. Nakamichi et al. constructed an *Mkx*$^{-/-}$ mouse model and discovered that TGF-β signaling pathway plays an important role in the development of outer AF [57]. In this study, we observed a malformed AF along with the transformation of fibroblast-like cells to chondrocyte-like cells in the AF of *Fam20B*–deficient mice. Taken together, we speculated that FAM20B may play an important role in the development of AF via the regulation of TGF-β signaling pathways. To test these postulates, we assessed the TGF-β signaling pathways in the AF of cKO mice versus normal control mice.

In the AF of cKO mice, the levels of phospho-Smad 2 and phospho-Smad 3, two main participants of the canonical TGF-β signaling pathway, were significantly lower, indicating that the Smad-dependent TGF-β signaling pathway was inhibited in the AF of *Fam20B*-deficient mice. Furthermore, we examined SCX, a marker of AF tissue and a downstream target of canonical TGF-β signaling pathway, which is regulated positively by Smad 2 and Smad 3 [62]. We observed that both the protein and the mRNA levels of SCX were significantly reduced in AF of cKO mice. These results indicate that the functional loss of FAM20B strongly inhibits the activation of TGF-β signaling pathway.

We also examined the levels of JNK, P38 and ERK, the key players of MAPK signaling pathways [63]. In the AF of cKO mice, we observed a remarkably down-regulated activation of the MAPK-JNK pathway. Ulici et al. constructed a *JNK1/2* double knockout mouse model and found that MAPK-JNK signaling pathway plays an important role in the development of AF [64]; the malformed AF in cKO mice may be, in part, due to the downregulation of JNK/MAPK pathway caused by inactivation of FAM20B. Studies have also shown that MAPK-JNK pathway inhibits the expressions of chondrocyte markers, such as Sox 9 and type II collagen [65,66]. In this study, the inhibition of MAPK-JNK pathway associated with the inactivation of FAM20B may be one of the factors that increased the expression levels of Sox 9 and type II collagen, contributing to cartilage metaplasia of outer AF. The levels of phosphorylated P38 and ERK were significantly elevated in the AF of cKO mice, suggesting that the inactivation of FAM20B may have activated the MAPK-P38/MAPK-ERK pathways in AF. As the altered activation of MAPK signaling pathways may induce improper differentiation of AF cells into chondrocytes [31,67], it is possible that changes in the levels of phosphorylated P38 and ERK may also contribute to the cell fate change in the AF of cKO mice.

5. Conclusion

This is the first report regarding the roles of FAM20B in the development of AF. Our findings show that FAM20B is essential to the development of AF in IVD and this enzyme may regulate the development of AF in IVD via TGF-β and MAPK signaling pathways. The *Fam20B* knock out mouse model may serve as a useful animal model to study the molecular mechanisms of AF development.

Supplementary data to this article can be found online at https://doi.org/10.1016/j.bbadis.2019.165555.

Transparency document

The Transparency document associated with this article can be found, in online version.

Declaration of competing interest

The authors declared that they have no conflicts of interest to this work.

Acknowledgements

This work was supported by USA National Institutes of Health Grant DE022549.

References

[1] Ma K, Chen S, Li Z, Deng X, Huang D, Xiong L, Shao Z. Mechanisms of endogenous repair failure during intervertebral disc degeneration. Osteoarthr. Cartil. 2019 Jan; 27(1):41–48. doi:https://doi.org/10.1016/j.joca.2018.08.021. PMID: 30243946.
[2] C. Feng, M. Yang, M. Lan, C. Liu, Y. Zhang, B. Huang, H. Liu, Y. Zhou, ROS: crucial intermediators in the pathogenesis of intervertebral disc degeneration, Oxidative Med. Cell. Longev. 2017 (2017) 5601593–5601605, https://doi.org/10.1155/2017/5601593 (28392887).
[3] Wu Q, Mathers C, Wang EW, Sheng S, Wenkert D, Huang JH. TGF-β initiates β-catenin-mediated CTGF secretory pathway in old bovine nucleus pulposus cells: a potential mechanism for intervertebral disc degeneration. JBMR Plus. 2018 Jul 10; 3(2):e10069. doi:https://doi.org/10.1002/jbm4.10069. PMID: 30828686.
[4] Gao C, Ning B, Sang C, Zhang Y. Rapamycin prevents the intervertebral disc degeneration via inhibiting differentiation and senescence of annulus fibrosus cells. Aging (Albany NY) 2018 Jan 18; 10(1):131–143. doi: 10.18632/aging.101364. PMID: 29348392.
[5] Zehra U, Cheung JPY, Bow C, Lu W, Samartzis D. Multidimensional vertebral endplate defects are associated with disc degeneration, modic changes, facet joint abnormalities, and pain. J. Orthop. Res. 2019 May; 37(5):1080–1089. doi:https://doi.org/10.1002/jor.24195. PMID: 30515862.
[6] Wang X, Wang B, Zou M1, Li J, Lü G, Zhang Q1, Liu F, Lu C. CircSEMA4B targets miR-431 modulating IL-1β-induced degradative changes in nucleus pulposus cells in intervertebral disc degeneration via Wnt pathway. Biochim. Biophys. Acta Mol. basis Dis. 2018 Nov; 1864(11):3754–3768. doi:https://doi.org/10.1016/j.bbadis.2018.08.033. PMID: 30251693.
[7] Y. Tan, X. Yao, Z. Dai, Y. Wang, G. Lv, Bone morphogenetic protein 2 alleviated intervertebral disc degeneration through mediating the degradation of ECM and apoptosis of nucleus pulposus cells via the PI3K/Akt pathway, Int. J. Mol. Med. 43 (1) (2019 Jan) 583–592, https://doi.org/10.3892/ijmm.2018.3972. PMID: 30387830.
[8] S. Munir, M.B. Freidin, M. Rade, J. Määttä, G. Livshits, F.M.K. Williams, Endplate defect is heritable, associated with low back pain and triggers intervertebral disc degeneration: a longitudinal study from TwinsUK, Spine (Phila Pa 1976) 43 (21) (2018 Nov 1) 1496–1501, https://doi.org/10.1097/BRS.0000000000002721 (29847371).
[9] Louie PK, Espinoza Orías AA, Fogg LF, LaBelle M, An HS, Andersson GBJ, Nozomu Inoue. Changes in lumbar endplate area and concavity associated with disc degeneration. Spine (Phila Pa 1976). 2018 Oct 1; 43(19):E1127-E1134. doi:https://doi.org/10.1097/BRS.0000000000002657. PMID: 29596278.
[10] Jill PG Urban, Sally Roberts. Degeneration of the intervertebral disc. Arthritis Res Ther. 2003; 5(3): 120–130. doi:https://doi.org/10.1186/ar629. PMID: 12723977.
[11] Min Ho Hwang, Hyeong Guk Son, Jae Won Lee, Chang Min Yoo, Jae Hee Shin, Hyo Geun Nam, Hyun Jung Lim, Seung Min Baek, Jeong Hun Park, Joo Han Kim, Hyuk Choi. Photobiomodulation of extracellular matrix enzymes in human nucleus pulposus cells as a potential treatment for intervertebral disk degeneration. Sci. Rep. 2018; 8: 11654–11658. doi:https://doi.org/10.1038/s41598-018-30185-3. PMID: 30076336.

[12] Po-Hsin Chou, Shih-Tien Wang, Meng-Hua Yen, Chien-Lin Liu, Ming-Chau Chang, Oscar Kuang-Sheng Lee. Fluid-induced, shear stress-regulated extracellular matrix and matrix metalloproteinase genes expression on human annulus fibrosus cells. Stem Cell Res Ther. 2016 Feb 27; 7: 34–42. doi:https://doi.org/10.1186/s13287-016-0292-5. PMID: 26921206.
[13] Aldemar Andres Hegewald, Jessie Cluzel, Jan Philipp Krüger, Michaela Endres, Christian Kaps, Claudius Thomé. Effects of initial boost with TGF-beta 1 and grade of intervertebral disc degeneration on 3D culture of human annulus fibrosus cells. J. Orthop. Surg. Res. 2014 Aug 14; 9: 73–82. doi:https://doi.org/10.1186/s13018-014-0073-8. PMID: 25116605.
[14] J E Scott, T R Bosworth, A M Cribb, J R Taylor. The chemical morphology of age-related changes in human intervertebral disc glycosaminoglycans from cervical, thoracic and lumbar nucleus pulposus and annulus fibrosus. J. Anat. 1994 Feb; 184(Pt 1): 73–82. PMID: 8157495.
[15] Melrose J, Ghosh P, Taylor TK. A comparative analysis of the differential spatial and temporal distributions of the large (aggrecan, versican) and small (decorin, biglycan, fibromodulin) proteoglycans of the intervertebral disc. J. Anat. 2001 Jan; 198(Pt 1):3–15. PMID: 11215765.
[16] Estelle C Collin, Oliver Carroll, Michelle Kilcoyne, Marianna Peroglio, Eugene See, Doris Hendig, Mauro Alini, Sibylle Grad, Abhay Pandit. Ageing affects chondroitin sulfates and their synthetic enzymes in the intervertebral disc. Signal Transduct Target Ther. 2017 Sep 22; 2: 17049–17057. doi:https://doi.org/10.1038/sigtrans.2017.49. PMID: 29263929.
[17] Zhang H, Zhu Q, Cui J, Wang Y, Chen MJ, Guo X, Tagliabracci VS, Dixon JE, Xiao J. Structure and evolution of the Fam20 kinases. Nat. Commun. 2018 Mar 23; 9(1):1218–1230. doi:https://doi.org/10.1038/s41467-018-03615-z. PMID: 29572475.
[18] Wen J, Xiao J, Rahdar M, Choudhury BP, Cui J, Taylor GS, Esko JD, Dixon JE. Xylose phosphorylation functions as a molecular switch to regulate proteoglycan biosynthesis. Proc. Natl. Acad. Sci. U. S. A. 2014 Nov 4; 111(44):15723–15728. doi:https://doi.org/10.1073/pnas.1417993111. PMID: 20556869.
[19] Koike T, Izumikawa T, Sato B, Kitagawa H. Identification of phosphatase that dephosphorylates xylose in the glycosaminoglycan-protein linkage region of proteoglycans. J. Biol. Chem. 2014 Mar 7; 289(10):6695–6708. doi:https://doi.org/10.1074/jbc.M113.520536. PMID: 24425863.
[20] Vogel P, Hansen GM, Read RW, Vance RB, Thiel M, Liu J, Wronski TJ, Smith DD, Jeter-Jones S, Brommage R. Amelogenesis imperfecta and other biomineralization defects in Fam20a and Fam20c null mice. Vet. Pathol. 2012 Nov; 49(6):998–1017. doi:https://doi.org/10.1177/0300985812453177. PMID: 22732358.
[21] Tian Y, Ma P, Liu C, Yang X, Crawford DM, Yan W, Bai D, Qin C, Wang X. Inactivation of Fam20B in the dental epithelium of mice leads to supernumerary incisors. Eur. J. Oral Sci. 2015 Dec; 123(6):396–402. doi:https://doi.org/10.1111/eos.12222. PMID: 26465965.
[22] Ma P, Yan W, Tian Y, Wang J, Feng JQ, Qin C, Cheng YS, Wang X. Inactivation of Fam20B in joint cartilage leads to chondrosarcoma and postnatal ossification defects. Sci. Rep. 2016 Jul 13; 6:29814–29826. doi:https://doi.org/10.1038/srep29814. PMID: 27405802.
[23] Wu MY, Hill CS. Tgf-beta superfamily signaling in embryonic development and homeostasis. Dev. Cell 2009 Mar; 16(3):329–343. doi:https://doi.org/10.1016/j.devcel.2009.02.012. PMID: 19289080.
[24] Michael O. Baffi, Molly A. Moran, Rosa Serra. Tgfbr2 regulates the maintenance of boundaries in the axial skeleton. Dev. Biol. 2006 Aug 15; 296(2): 363–374. doi:https://doi.org/10.1016/j.ydbio.2006.06.002. PMID: 16824508.
[25] Baffi MO, Slattery E, Sohn P, Moses HL, Chytil A, Serra R. Conditional deletion of the TGF-beta type II receptor in Col2a expressing cells results in defects in the axial skeleton without alterations in chondrocyte differentiation or embryonic development of long bones. Dev. Biol. 2004 Dec 1; 276(1):124–142. DOI:https://doi.org/10.1016/j.ydbio.2004.08.027. PMID: 15531369.
[26] Alkhatib B, Liu C, Serra R. Tgfbr2 is required in Acan-expressing cells for maintenance of the intervertebral and sternocostal joints. JOR Spine. 2018 Jun 22; 1(2). pii: e1025-e1048. doi:https://doi.org/10.1002/jsp2.1025. PMID: 30662980.
[27] P.H. Chou, S.T. Wang, H.L. Ma, C.L. Liu, M.C. Chang, O.K. Lee, Development of a two-step protocol for culture expansion of human annulus fibrosus cells with TGF-β1 and FGF-2, Stem Cell Res Ther 7 (1) (2016 Jul 12) 89–98, https://doi.org/10.1186/s13287-016-0332-1 (27405858).
[28] Kurtzeborn K, Kwon HN, Kuure S. MAPK/ERK signaling in regulation of renal differentiation. Curr Biol. Int J Mol Sci. 2019 Apr 10; 20(7). pii: E1779-E1789. doi:https://doi.org/10.3390/ijms20071779. PMID: 30974877.
[29] Kim MY, Choi TY, Kim JH, Lee JH, Kim JG, Sohn KC, Yoon KS, Kim CD, Lee JH, Yoon TJ. MKK6 increases the melanocyte dendricity through the regulation of Rho family GTPases. J. Dermatol. Sci. 2010 Nov; 60(2):114–129. doi:https://doi.org/10.1016/j.jdermsci.2010.08.006. PMID: 20869211.
[30] Zhang K, Ding W, Sun W, Sun XJ, Xie YZ, Zhao CQ, Zhao J. Beta1 integrin inhibits apoptosis induced by cyclic stretch in annulus fibrosus cells via ERK1/2 MAPK pathway. Apoptosis. 2016 Jan; 21(1):13–24. doi:https://doi.org/10.1007/s10495-015-1180-7. PMID: 26467923.
[31] Ding W1, Zhao C, Cao L, Zhang K, Sun W, Xie Y, Li H, Zhao J. Leptin induces terminal differentiation of rat annulus fibrosus cells via activation of MAPK signaling. Anat Rec (Hoboken). 2013 Dec; 296(12):1806–1812. doi:https://doi.org/10.1002/ar.22806. PMID: 24249395.
[32] S. Hirose, K. Narita, K. Asano, A. Nakane, Salmon cartilage proteoglycan promotes the healing process of Staphylococcus aureus-infected wound, Heliyon. 4 (3) (2018 Mar 27) e00587-e00599, , https://doi.org/10.1016/j.heliyon.2018.e00587 (29862350).
[33] Zamani S, Hashemibeni B, Esfandiari E, Kabiri A, Rabbani H, Abutorabi R. Assessment of TGF-β3 on production of aggrecan by human articular chondrocytes in pellet culture system. Adv Biomed Res. 2014 Jan 27; 3:54–62. doi:https://doi.org/10.4103/2277-9175.125799. PMID: 24627862.
[34] Thouverey C, Caverzasio J. Focus on the p38 MAPK signaling pathway in bone development and maintenance. Bonekey Rep. 2015 Jun 10; 4:711–719. doi:https://doi.org/10.1038/bonekey.2015.80. PMID: 26131361.
[35] B.F. Eames, Y.L. Yan, M.E. Swartz, D.S. Levic, E.W. Knapik, J.H. Postlethwait, C.B. Kimmel, Mutations in fam20b and xylt1 reveal that cartilage matrix controls timing of endochondral ossification by inhibiting chondrocyte maturation, PLoS Genet. 7 (8) (2011 Aug) e1002246-e1002258, , https://doi.org/10.1371/journal.pgen.1002246. PMID: 21901110.
[36] T. Wang, F. Yang, A comparative study of chondroitin sulfate and heparan sulfate for directing three-dimensional chondrogenesis of mesenchymal stem cells, Stem Cell Res Ther 8 (1) (2017 Dec 19) 284–292, https://doi.org/10.1186/s13287-017-0728-6 (29258589).
[37] Schindewolf M, Steindl J, Beyer-Westendorf J, Schellong S, Dohmen PM, Brachmann J, Madlener K, Pötzsch B, Klamroth R, Hankowitz J, Banik N, Eberle S, Müller MM, Kropff S, Lindhoff-Last E. Use of fondaparinux off-label or approved anticoagulants for management of heparin-induced thrombocytopenia. J. Am. Coll. Cardiol. 2017 Nov 28; 70(21):2636–2648. doi:https://doi.org/10.1016/j.jacc.2017.09.1099. PMID: 29169470.
[38] H. Zhang, X. Xie, P. Liu, T. Liang, Y. Lu, C. Qin, Transgenic expression of dentin phosphoprotein (DPP) partially rescued the dentin defects of DSPP-null mice, PLoS One 13 (4) (2018 Apr 19) e0195854–e0195863, https://doi.org/10.1371/journal.pone.0195854 (29672573).
[39] P. Liu, S. Ma, H. Zhang, C. Liu, Y. Lu, L. Chen, C. Qin, Specific ablation of mouse Fam20C in cells expressing type I collagen leads to skeletal defects and hypophosphatemia, Sci. Rep. 7 (1) (2017 Jun 15) 3590–3599, https://doi.org/10.1038/s41598-017-03960-x (28620244).
[40] Lin S, Zhang Q, Cao Z, Lu Y, Zhang H, Yan K, Liu Y, McKee MD, Qin C, Chen Z, Feng JQ. Constitutive nuclear expression of dentin matrix protein 1 fails to rescue the Dmp1-null phenotype. J. Biol. Chem. 2014 Aug 1; 289(31):21533–21543. doi:https://doi.org/10.1074/jbc.M113.543330. PMID: 24917674.
[41] Liu C, Zhou N, Wang Y, Zhang H, Jani P, Wang X, Lu Y, Li N, Xiao J, Qin C. Abrogation of Fam20c altered cell behaviors and BMP signaling of immortalized dental mesenchymal cells. Exp. Cell Res. 2018 Feb 15; 363(2):188–195. doi:https://doi.org/10.1016/j.yexcr.2018.01.004. PMID: 29337188.
[42] Min Li, Manda Sai Krishnaveni, Changgong Li, Beiyun Zhou, Yiming Xing, Agnes Banfalvi, Aimin Li, Vincent Lombardi, Omid Akbari, Zea Borok, Parviz Minoo. Epithelium-specific deletion of TGF-β receptor type II protects mice from bleomycin-induced pulmonary fibrosis. J. Clin. Invest. 2011 Jan 4; 121(1): 277–287. doi:https://doi.org/10.1172/JCI42090. PMID: 21135509.
[43] Bau-Lin Huang, Sean M. Brugger, Karen M. Lyons. Stage-specific control of connective tissue growth factor (CTGF/CCN2) expression in chondrocytes by Sox 9 and β-catenin. J. Biol. Chem. 2010 Sep 3; 285(36): 27702–27712. doi:https://doi.org/10.1074/jbc.M110.108498. PMID: 20571031.
[44] Takimoto A, Kawatsu M, Yoshimoto Y, Kawamoto T, Seiryu M, Takano-Yamamoto T, Hiraki Y, Shukunami C. Scleraxis and osterix antagonistically regulate tensile force-responsive remodeling of the periodontal ligament and alveolar bone. Development. 2015 Feb 15; 142(4):787–796. doi:https://doi.org/10.1242/dev.116228. PMID: 25670797.
[45] Priyam H. Jani, Monica P. Gibson, Chao Liu, Hua Zhang, Xiaofang Wang, Yongbo Lu, Chunlin Qin. Transgenic expression of Dspp partially rescued the long bone defects of Dmp1-null mice. Matrix Biol. 2016 May-Jul; 52-54: 95–112. doi:https://doi.org/10.1016/j.matbio.2015.12.001. PMID: 26686820.
[46] J. Zieba, K.N. Forlenza, J.S. Khatra, A. Sarukhanov, I. Duran, D. Rigueur, K.M. Lyons, D.H. Cohn, A.E. Merrill, D. Krakow, TGFβ and BMP dependent cell fate changes due to loss of filamin B produces disc degeneration and progressive vertebral fusions, PLoS Genet. 12 (3) (2016 Mar 28) e1005936–e1005958, https://doi.org/10.1371/journal.pgen.1005936 (27019229).
[47] J.I. Sive, P. Baird, M. Jeziorsk, A. Watkins, J.A. Hoyland, A.J. Freemont, Expression of chondrocyte markers by cells of normal and degenerate intervertebral discs, Mol. Pathol. 55 (2) (2002 Apr) 91–97, https://doi.org/10.1136/mp.55.2.91. PMID: 11950957.
[48] Wu M, Chen G, Li YP. TGF-β and BMP signaling in osteoblast, skeletal development, and bone formation, homeostasis and disease. Bone Res. 2016 Apr 26; 4:16009–16030. doi:https://doi.org/10.1038/boneres.2016.9. PMID: 27563484.
[49] Berthet E, Chen C, Butcher K, Schneider RA, Alliston T, Amirtharajah M. Smad3 Binds Scleraxis and Mohawk and Regulates Tendon Development. J Orthop Res. 2013 Sep; 31(9): 1475–1483. doi: 10.1002/jor.22382. PMID: 23653374.
[50] Zhang YE. Non-Smad pathways in TGF-beta signaling. Cell Res. 2009 Jan; 19(1):128–139. doi:https://doi.org/10.1038/cr.2008.328. PMID: 19114990.
[51] J.C. Lotz, J.R. Chin, Intervertebral disc cell death is dependent on the magnitude and duration of spinal loading, Spine (Phila Pa 1976) 25 (12) (2000 Jun 15) 1477–1483 (10851095).
[52] J.C. Iatridis, P.L. Mente, I.A. Stokes, D.D. Aronsson, M. Alini, Compression-induced changes in intervertebral disc properties in a rat tail model, Spine (Phila Pa 1976) 24 (10) (1999 May 15) 996–1002 (10332792).
[53] Chan SC, Ferguson SJ, Gantenbein-Ritter B. The effects of dynamic loading on the intervertebral disc. Eur. Spine J. 2011 Nov; 20(11):1796–1812. doi:https://doi.org/10.1007/s00586-011-1827-1. PMID: 21541667.
[54] Ishihara H, McNally DS, Urban JP, Hall AC. Effects of hydrostatic pressure on matrix synthesis in different regions of the intervertebral disk. J Appl Physiol (1985). 1996 Mar; 80(3):839–46. DOI:https://doi.org/10.1152/jappl.1996.80.3.839. PMID: 8964745.
[55] Ban GI, Williams S, Serra R. Antagonism of BMP signaling is insufficient to induce fibrous differentiation in primary sclerotome. Exp. Cell Res. 2019 May 1;

378(1):11–20. doi:https://doi.org/10.1016/j.yexcr.2019.01.026. PMID: 30817928.
[56] Williams S, Alkhatib B, Serra R. Development of the axial skeleton and intervertebral disc. Curr. Top. Dev. Biol. 2019; 133:49–90. doi:https://doi.org/10.1016/bs.ctdb.2018.11.018. PMID: 30902259.
[57] Nakamichi R, Ito Y, Inui M, Onizuka N, Kayama T, Kataoka K, Suzuki H, Mori M, Inagawa M, Ichinose S, Lotz MK, Sakai D, Masuda K, Ozaki T, Asahara H. Mohawk promotes the maintenance and regeneration of the outer annulus fibrosus of intervertebral discs. Nat. Commun. 2016 Aug 16; 7:12503–12517. doi:https://doi.org/10.1038/ncomms12503. PMID: 27527664.
[58] Liu X, Krishnamoorthy D, Lin L, Xue P, Zhang F, Chi L, Linhardt RJ, Iatridis JC. A method for characterising human intervertebral disc glycosaminoglycan disaccharides using liquid chromatography-mass spectrometry with multiple reaction monitoring. Eur Cell Mater. 2018 Feb 22; 35:117–131. doi: 10.22203/eCM.v035a09. PMID: 29469163.
[59] Hondke S, Cabraja M, Krüger JP, Stich S, Hartwig T, Sittinger M, Endres M. Proliferation, migration, and ECM formation potential of human annulus fibrosus cells is independent of degeneration status. Cartilage. 2018 Mar 1:1947603518764265. doi:https://doi.org/10.1177/1947603518764265. PMID: 29577749.
[60] E.S. Silagi, I.M. Shapiro, M.V. Risbud. Glycosaminoglycan synthesis in the nucleus pulposus: dysregulation and the pathogenesis of disc degeneration. Matrix Biol. 2018 Oct; 71-72:368–379. doi:https://doi.org/10.1016/j.matbio.2018.02.025. PMID: 29501510.
[61] Sohn P, Cox M, Chen D, Serra R. Molecular profiling of the developing mouse axial skeleton: a role for Tgfbr2 in the development of the intervertebral disc. BMC Dev. Biol. 2010 Mar 9; 10:29–44. doi:https://doi.org/10.1186/1471-213X-10-29. PMID: 20214815.
[62] Maeda T, Sakabe T, Sunaga A, Sakai K, Rivera AL, Keene DR, Sasaki T, Stavnezer E, Iannotti J, Schweitzer R, Ilic D, Baskaran H, Sakai T. Conversion of mechanical force into TGF-β-mediated biochemical signals. Curr. Biol. 2011 Jun 7; 21(11):933–941. doi:https://doi.org/10.1016/j.cub.2011.04.007. PMID: 21600772.
[63] Turner NA, Blythe NM. Cardiac fibroblast p38 MAPK: a critical regulator of myocardial remodeling. J Cardiovasc Dev Dis. 2019 Aug 7; 6(3):27–45. doi:https://doi.org/10.3390/jcdd6030027. PMID: 31394846.
[64] Ulici V, Kelley KL, Longobardi L, McNulty MA, Livingston EW, Bateman TA, Séguin CA, Louer CR, Loeser RF. Impaired annulus fibrosus development and vertebral fusion cause severe scoliosis in mice with deficiency of c-Jun NH2-terminal kinases 1 and 2. Am. J. Pathol. 2019 Apr; 189(4):868–885. doi:https://doi.org/10.1016/j.ajpath.2018.12.010. PMID: 30664861.
[65] Nakajima M, Negishi Y, Tanaka H, Kawashima K. p21 (Cip-1/SDI-1/WAF-1) expression via the mitogen-activated protein kinase signaling pathway in insulin-induced chondrogenic differentiation of ATDC5 cells. Biochem. Biophys. Res. Commun. 2004 Aug 6; 320(4):1069–1075. doi:https://doi.org/10.1016/j.bbrc.2004.06.057. PMID: 15249198.
[66] Hwang SG, Yu SS, Poo H, Chun JS. c-Jun/activator protein-1 mediates interleukin-1beta-induced dedifferentiation but not cyclooxygenase-2 expression in articular chondrocytes. J. Biol. Chem. 2005 Aug 19; 280(33):29780–29787. PMID: 15961395.
[67] Daniels J, Binch AA, Le Maitre CL. Inhibiting IL-1 signaling pathways to inhibit catabolic processes in disc degeneration. J. Orthop. Res. 2017 Jan; 35(1):74–85. doi:https://doi.org/10.1002/jor.23363.. PMID: 27391542.